NUREG/CR-4034

A Study of Droplet Hydrodynamics Across a Grid Spacer

Prepared by S. L. Lee, S. K. Cho, H. J. Sheen

College of Engineering and Applied Sciences
State University of New York at Stony Brook

Prepared for
U.S. Nuclear Regulatory
Commission

GPO Printed copy price: $4.50

NUREG/CR-4034
R2

A Study of Droplet Hydrodynamics Across a Grid Spacer

Manuscript Completed: February 1984
Date Published: November 1984

Prepared by
S. L. Lee, S. K. Cho, H. J. Sheen

College of Engineering and Applied Sciences
State University of New York at Stony Brook
Stony Brook, NY 11794

Prepared for
Division of Accident Evaluation
Office of Nuclear Regulatory Research
U.S. Nuclear Regulatory Commission
Washington, D.C. 20555
Under Contract No. NRC G-04-81-014

ABSTRACT

In this report, the results of measurement of droplet size and velocity upstream and downstream of the grid spacer are reported. All experiments were performed at ambient atmospheric pressure and room temperature. The LDA system was used for simultaneous measurement of size and velocity of a droplet, and at every measurement location two size measurement schemes were employed. These measurement results show that some of the thermally inactive large droplets (>1mm) are intercepted by the grid spacer and broken down to thermally more active smaller droplets (<100μ) after the grid spacer. From the obtained data, Sauter mean diameter and area density were calculated. The correlations on the Sauter mean diameter of the large and small droplets downstream of the grid spacer are reported. Also correlations on the fractional volume of the small droplets and nozzle characteristics are reported respectively. These results show that after liquid droplets' breakage, the total surface area of the droplets is greatly increased. This phenomenon will lead to enhanced cooling of fuel rods in nuclear reactor during reflood for a postulated large loss of coolant accident.

TABLE OF CONTENTS

LIST OF FIGURES

LIST OF FIGURES

LIST OF TABLES

ACKNOWLEDGEMENTS

The authors would like to acknowledge the support of the U. S. Nuclear Regulatory Commission for its support (NRC Grant No: 473-5184) which has made this investigation possible. They would also like to express their thanks to Dr.'s M. Young and R. Lee for their guidance and assistance in the work and to Mrs. L. Infranco for her help in the preparation of this report. In addition, the Institut für Reaktorbauelemente of the Kernforschungszentrum Karlsruhe (KfK), West Germany, is acknowledged for its generous supply of the KWU grid spacer.

NOMENCLATURE

$Area_{base}$	: Unit base area that one nozzle can cover.
$Area_{sc}$	: Considered total sub-channel area (area surrounded by solid line).
$Area_{gs}$	: Effective grid spacer area where supplied large liquid droplets are captured (area surrounded by dotted line).
$Area_{uo}$	: Unblocked area where supplied large liquid droplets are passing through without hitting the grid spacer. $Area_{uo} = Area_{sc} - Area_{gs}$
$\left(\frac{A_i}{V_t}\right)_1 = 6\frac{(1-\alpha)_1}{d_{sm_1}}$	: Interfacial area density at Location 1.
$\left(\frac{A_i}{V_t}\right)_{s,1} = \beta_{s,2}\left(\frac{A_i}{V_t}\right)_1$	: Fractional area density at Location 1 which corresponds to the volume of small droplets at Location 2.
$\left(\frac{A_i}{V_t}\right)_{L,1} = \beta_{L,2}\left(\frac{A_i}{V_t}\right)_1$	: Fractional area density at Location 1 which corresponds to the volume of large droplets at Location 2.
$\left(\frac{A_i}{V_t}\right)_{s,2}$ or $\left(\frac{A_i}{V_t}\right)_{L,2}$	: Interfacial area density of small or large droplets at Location 2.
$\left(\frac{A_i}{V_t}\right)_{s,2} \Big/ \left(\frac{A_i}{V_t}\right)_{s,1} = d_{sm_1} \Big/ d_{sms,2}$	: Ratio of area densities for the small droplets between Location 1 and Location 2.
$\left(\frac{A_i}{V_t}\right)_{L,2} \Big/ \left(\frac{A_i}{V_t}\right)_{L,1} = d_{sm_1} \Big/ d_{smL,2}$	: Ratio of area densities for the large droplets between Location 1 and Location 2.
$\left(\frac{A_i}{V_t}\right)_{s,2} \cdot V_{dL,1}$ or $\left(\frac{A_i}{V_t}\right)_{L,2} \cdot V_{dL,1}$	: Specific interfacial area flux for the small or large droplets at Location 2.

$\left(\frac{A_i}{V_t}\right)_{BGS}$: Interfacial area density before grid spacer.

$\left(\frac{A_i}{V_t}\right)_{AGS}$: Interfacial area density after grid spacer.

B : Systematic error.

B_{Cal} : Systematic error for calibration.

$B_{Data\ Acq}$: Systematic error for data acquisition.

B_{Meas} : Measured systematic error.

$d_{sm} = \frac{\int d^3 Ndd}{\int d^2 Ndd}$: Sauter mean diameter.

d_{sml} : Sauter mean diameter of liquid droplets which were measured at Location 1.

$d_{smL,2}$: Sauter mean diameter of large liquid droplets which were measured at Location 2.

$d_{sms,2}$: Sauter mean diameter of small liquid droplets which were measured at Location 2.

ℓ : Effective thickness of grid spacer which is a function of supplied droplet diameter.

Q_l : Water supply rate through 7 nozzles to a grid spacer.

S : Random error.

S_{Meas} : Measured Random error.

U : Uncertainty parameter.

U_A : Uncertainty for air velocity.

U_I : Interfacial area density uncertainty.

U_{Meas} : Uncertainty by the measurement.

U_Q : Uncertainty for flow rate (water).

U_{SMD} : Uncertainty for Sauter mean diameter.

U_V : Uncertainty for average droplet velocity

V_a : Air velocity in the channel.

V_{d_1} : Droplet velocity at Location 1.

x,y,z : Coordinates.

α : Void fraction

$(1-\alpha)_{s,1} = (1-\alpha)_1 \cdot \beta_{s,2}$: Fractional amount of the supplied water through Location 1 which corresponds to the volume of small droplets at Location 2.

$(1-\alpha)_{L,1} = (1-\alpha)_1 \cdot \beta_{L,2}$: Fractional amount of the supplied water through Location 1 which corresponds to the volume of large droplets at Location 2.

$\beta_{s,2} = \dfrac{(\int d^3 Ndd)_{s,2}}{(\int d^3 Ndd)_{s+L,2}}$: Fractional volume of the small liquid droplets in respect to the total liquid droplets volume at Location 2.

$\beta_{L,2} = \dfrac{(\int d^3 Ndd)_{L,2}}{(\int d^3 Ndd)_{s+L,2}}$: Fractional volume of the large liquid droplets at Location 2.

θ : Angle as defined in Figure B.2.

ω : Data rate.

1. INTRODUCTION

1.1 General

One of the NRC criteria for emergency core cooling systems of nuclear reactors is the prediction of the peak cladding temperature during the reflood phase of a PWR-LOCA. Under the United States code of federal regulations, "Each evaluation model should include provison for predicting cladding swelling and rupture from the consideration of the axial temperature distribution of the cladding, and from the difference in pressure between the inside and outside of the cladding, both as functions of time [1]." Ihle et al [2] reported a transient hydraulic experiment on the significant heat transfer mechanisms which are responsible for the development of the cladding temperature transient. These authors presented a typical measured cladding temperature transient near the top end of the heated bundle length compared with corresponding analytical predictions by two computer codes, RELAP4/MOD6 and REFLUX/GRS. The comparison reveals the inadequacy of the assumed heat transfer mechanisms in the analysis which results in significantly higher cladding temperature levels than measured during the initial period of reflooding.

During "bottom flooding", most evaluation-model and best-estimate codes model heat transfer from the hot, dry wall to a parallel vapor stream carrying droplets calculated by the critical Weber number [3] (~ few millimeters in size). Therefore, the cooling is calculated to be done primarily by convection to superheated steam without the presence of small droplets in the vapor flow. However, a sufficient population of smaller droplets usually serve as a very efficient cooling agent due to their large surface area to volume ratios. The thermally relatively inactive large droplets (>1mm) can be broken down to more active smaller droplets (<100μ) using grid spacers located at equal intervals along the entire length of the bundle [4]. Large droplets intercepted by each grid spacer produce a large number of small droplets downstream. The effect of this phenomenon is observed by a sharp dip of the cladding temperature just downstream of a grid spacer [5]. Hence, a direct verification of this suggested mechanism of droplet transformation of mist flow across the grid spacer plate is in order.

1.2 Task Objectives

The objectives of this task are to obtain experimental data and develop hydrodynamic correlations for the effect of grid spacers on mist flows. In details, the objectives are classified as follows:

a) Develop correlations to predict the rates of droplets re-entrainment in concurrent two-phase flow.
b) Develop correlations for predicting interfacial area density in dispersed flow regimes.
c) Provide data on droplet size distribution, droplet velocity and gas velocity.

2. FLOW ARRANGEMENTS AND EXPERIMENTAL SET-UP

The general arrangement of the experimental test rig is shown in a sketch (Figure 1). The flow channel is placed between a 15mW, He-Ne laser and photo-detectors. The flow channel is made of plexiglass with two glass windows. A 2x2 bundle of simulated glass rods of approximately 10.75mm outside diameter is put inside the channel. The total length of the flow channel is 1067mm. The glass rods are arranged with a pitch of 14.30mm. There are a total of three grid spacers, placed at 381mm intervals. The grid spacer is designed for the mist flow interference studies. The grid spacers are the standard vertical cross-plate design with a plate thickness of 0.5mm and a plate height of 38mm. Water droplets are supplied to the channel from seven (7) small nozzles. Water is supplied to a specially built distributor and then goes onto the nozzles. This way the pressure drop and flow rate are the same for all the operating nozzles. The setup of the nozzles is like the cross-plate design and they are placed 75mm below the middle grid spacer cross plates. During the experiment, the nozzles which are on a plane perpendicular to the laser beam are used. The nozzles are spaced at equal distance.

Compressed air is supplied through a honey-comb flow straightener from a compressed air line. Drainage ports are provided both at the top and bottom of the channel. Glass windows are needed for the passage of laser beams in the test section of the channel. But occasional blockage of the light beams by water droplets depositing on the inside surface of the window creates a serious problem. Introduction of the double-layered jacket window arrangement (Figure 2), cleaned by low pressure air, totally resolved this problem.

Measurements had been taken at two cross-sections, 5mm below and 22mm above the grid spacer. The location of the nozzles spraying water-droplets are shown in Figure 1. Figure 3 shows the effective grid spacer area, the center part of the flow subchannel where all the measurements have been taken. The effective thickness of the grid spacer, which is a function of supplied droplet diameter, was determined by a separate experiment.

3. OPTICAL TECHNIQUE AND INSTRUMENTATION

3.1 LDA System Arrangement and Methodology

The operational arrangement of the reference-mode laser-Doppler anemometer is shown in the sketch of Figure 4. The incoming laser beam from a 15mW He-Ne laser is split into two beams of unequal intensity, the weaker one for the reference beam and the stronger one for the scattering beam, which are then so polarized that they form at 45° polarization angle with each other. These beams are focussed by a focussing lens to the same point at an angle of 8.14 degrees to form a small measuring volume with a short dimension of about 240μm as shown in the sketch of Figure 4. Both the reference beam and the scattered light from the scattering beam on hitting a moving scattering body in the measuring volume

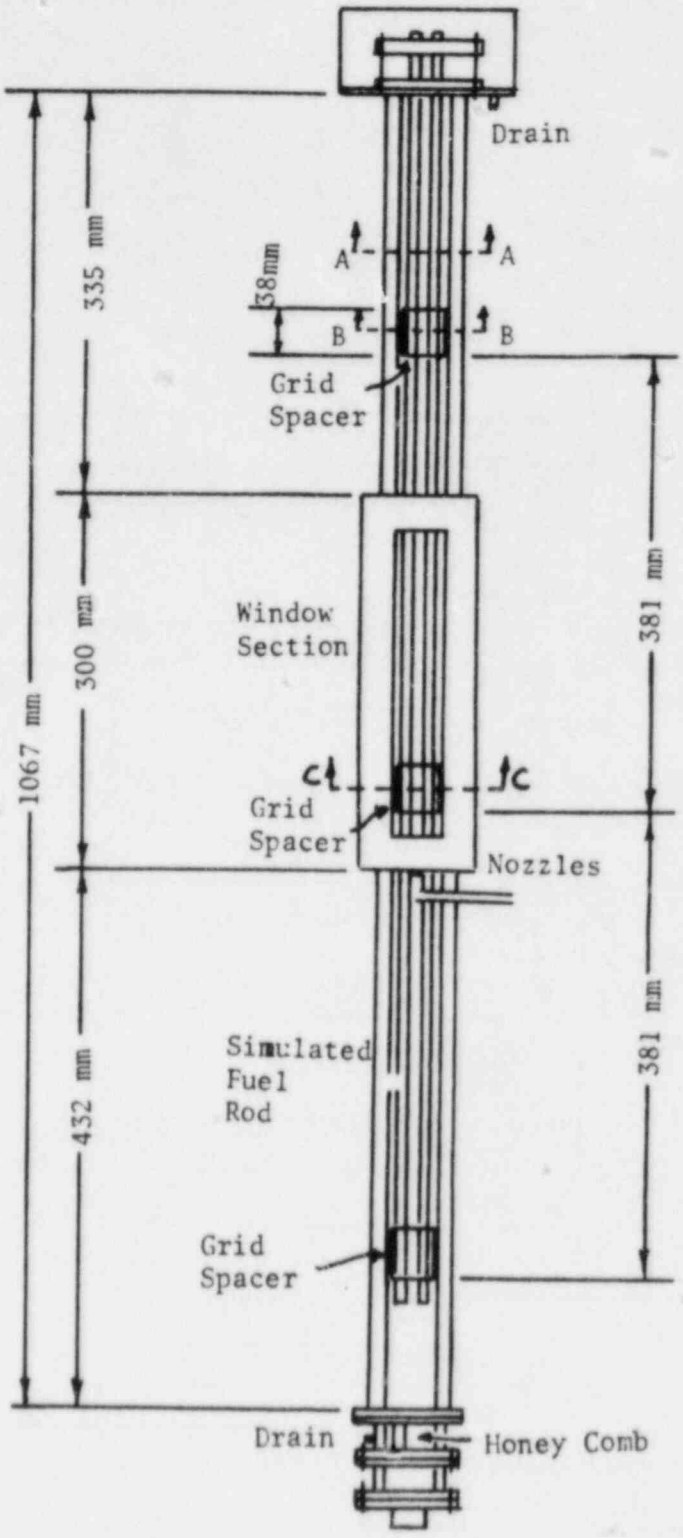

Figure 1. Channel.

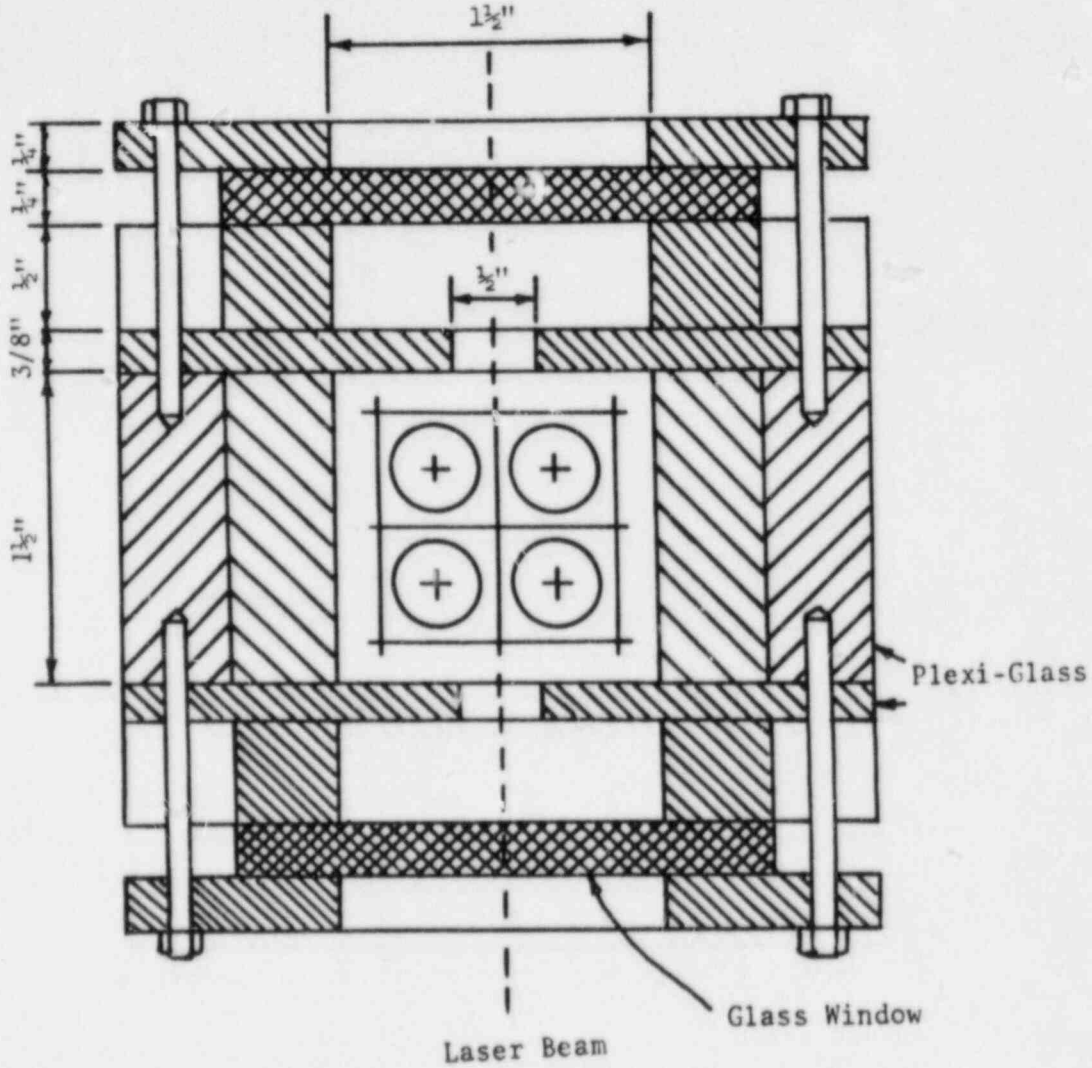

Figure 2. Cross section of the channel. (c-c)

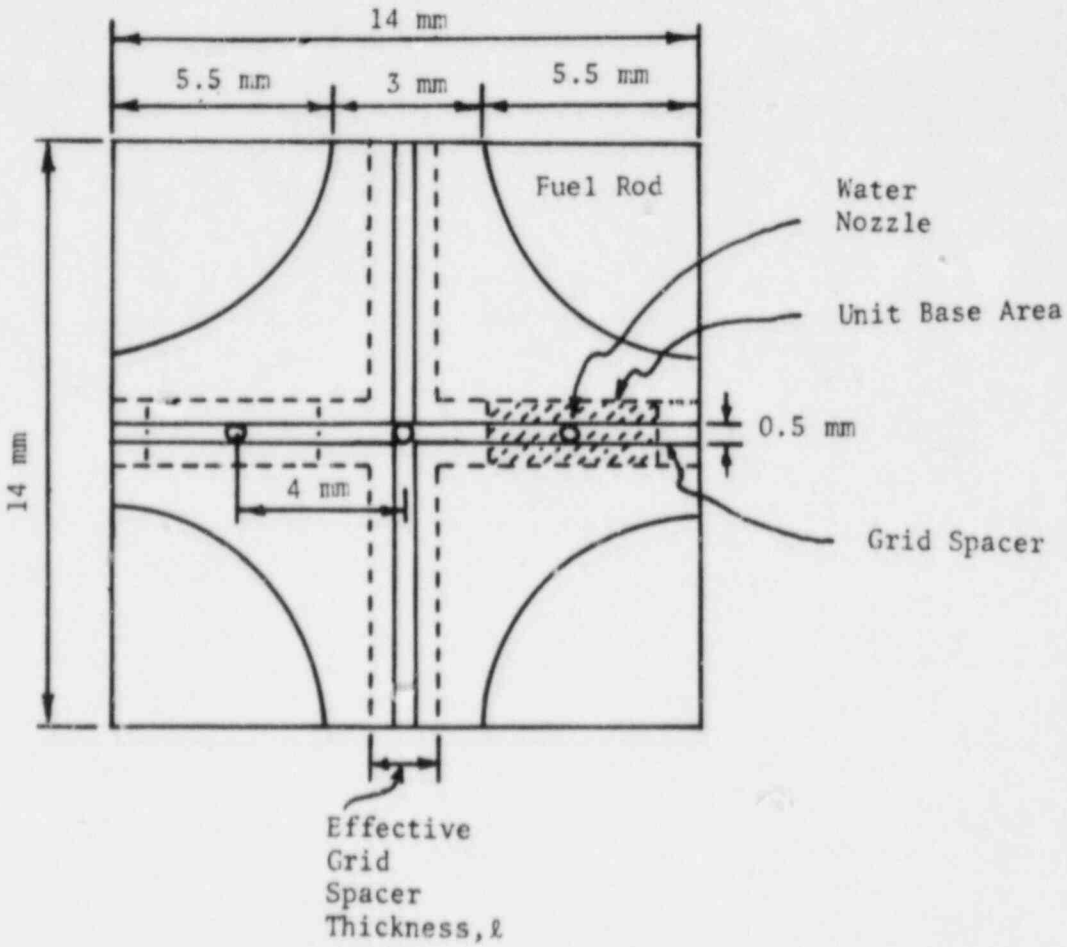

Figure 3. Geometry of effective grid spacer.

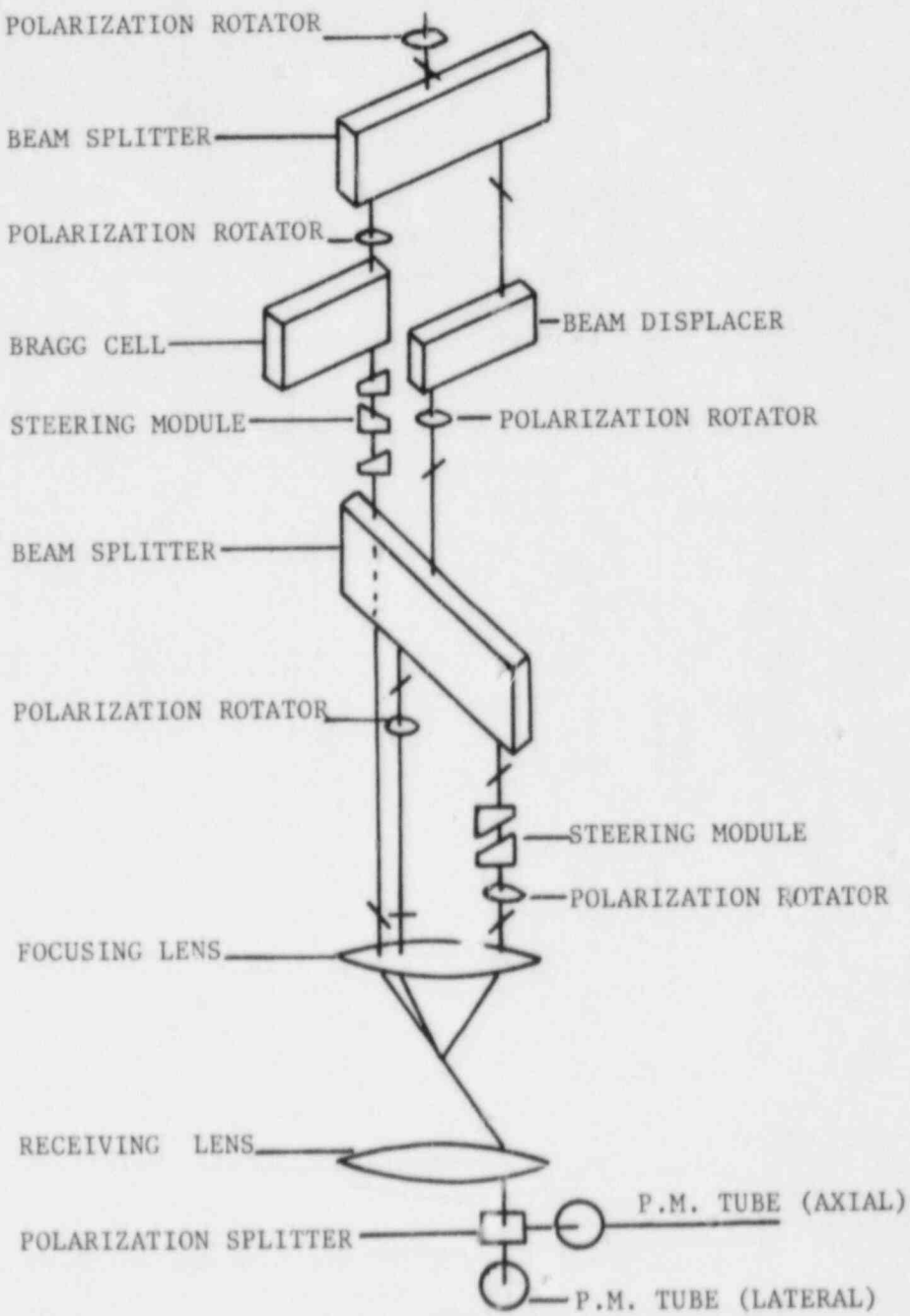

Figure 4. Optical Arrangement.

are picked up along the direction of the reference beam by a matching receiving lens. The received beam is then passed through a polarization splitter to be split into two beams, one with a polarization orientation the same as that of the scattering beam, and the other with a polarization orientation in the perpendicular direction. The beam with a polarization orientation the same as that of the scattering beam consists of the scattered beam and the component of the reference beam in the same polarization direction and is received through a small aperture by the photo-multiplier tube to produce the Doppler signal through heterodyning.

3.2 Large Particle Measurement Scheme

The beam with a polarization orientation perpendicu' to that of the scattering beam consists only of the components of .he reference beam in this direction and is received by a photo-diode for the purpose of measuring the size of the scattering body by measuring the time of blocking of the reference beam due to its cutting across the measuring volume. If there is no blocking of the reference beam, its two components, which are perpendicular to each other in orientation of polarization, excite the sensing elements of the photo-multipler tube and the photo-diode, respectively, resulting in added D.C. voltage outputs at both places. On the other hand, if there is blocking of the reference beam, these added D.C. voltage outputs at the photo-multiplier tube and the photo-diode will disappear and the voltage outputs will reflect the normal system electronic noise levels at these places. When a moving spherical particle of a size larger than the size of the reference beam cuts across the reference beam, the outputs of both the photo-multiplier tube and the photo-diode will show a drop from an elevated D.C. voltage to the system electronics noise voltage and after a drop-off period to be followed by a return to the same elevated D.C. voltage. This drop-off period represents the time taken for the center line of the reference beam to transverse across the circular area formed in its plane of intersection with the spherical particle. If this plane of intersection coincides with a vertical plane of symmetry of the spherical body, after the multiplication of a geometrical factor of the cosine of the small angle between the reference beam and the horizontal, this block-off period then represents the time taken for the spherical particle to move a distance of one length of its diameter at the same vertical velocity as outlined in the sketch of Figure 5. With a knowledge of the vertical velocity from the Doppler signal, one can then obtain the diameter of the spherical particle.

When the plane of intersection of the center line of the reference beam with the spherical particle lies within the smaller dimension of the optical measuring volume from the vertical axis of the particle and the point of detachment, which lies on the circular arch of intersect of the surface of the particle and a plane passing through the vertical axis of the particle and parallel to the reference beam, on leaving the reference beam lies within the larger dimension of the optical measuring volume, a Doppler signal is registered at the end of the block-off period as shown in Figure 6. The frequency of the Doppler signal gives the vertical

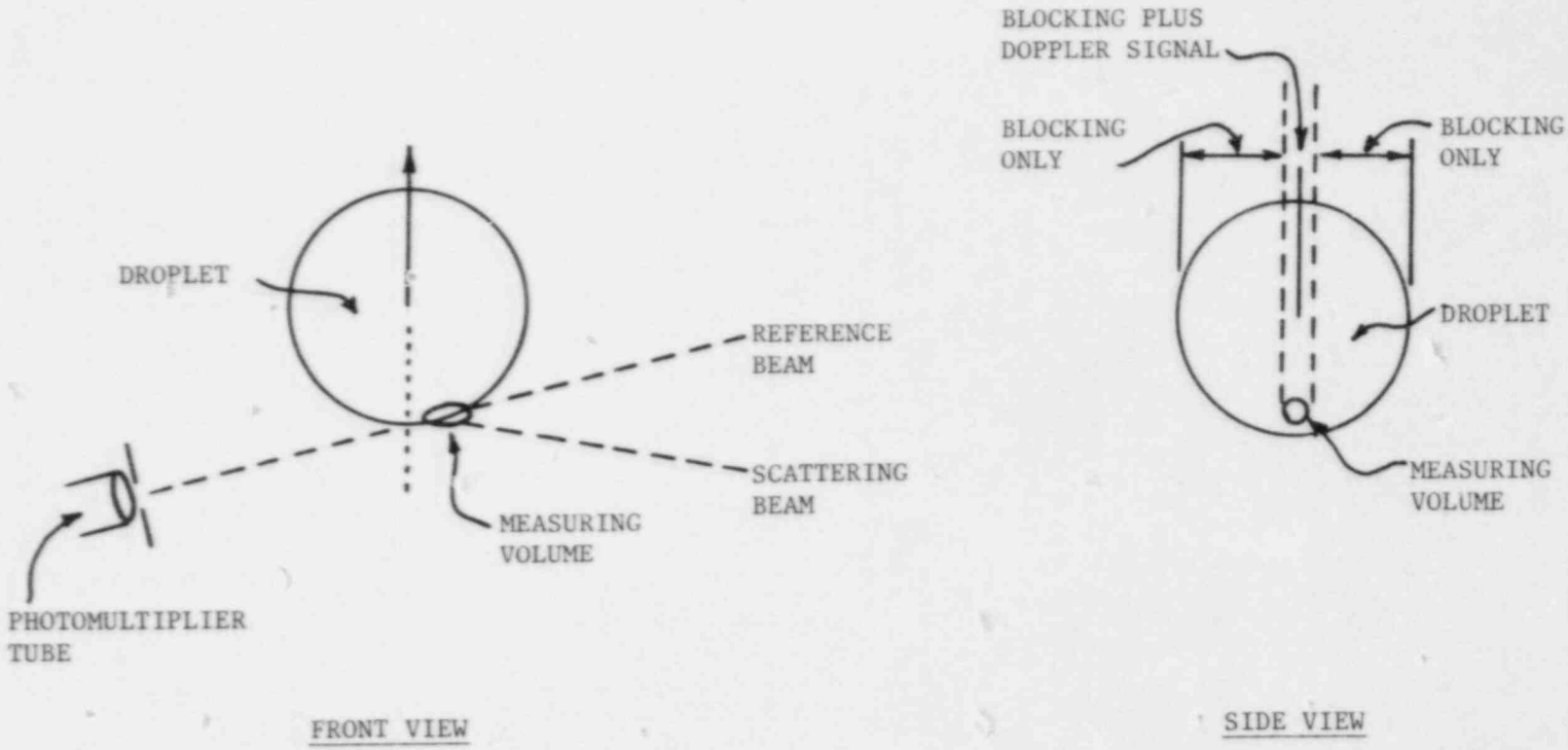

Figure 5. Laser-Doppler anemometry scheme developed for large-size droplet measurement.

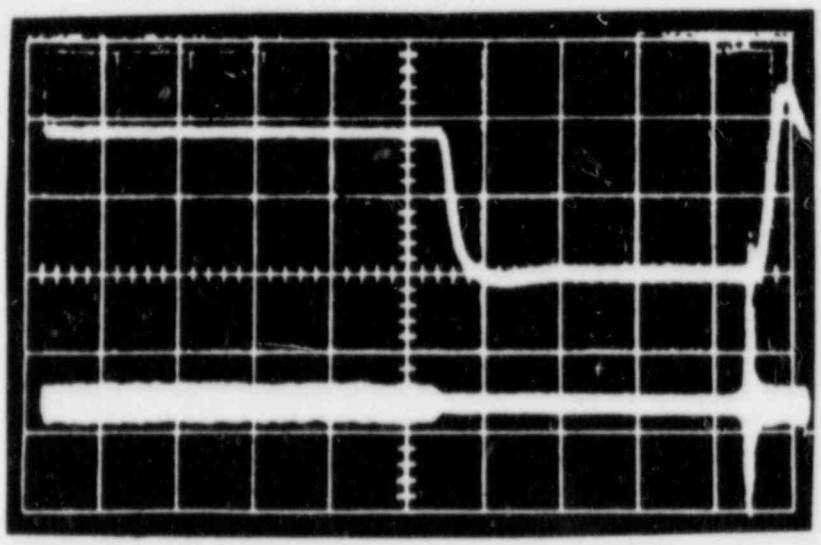

Figure 6. Photo-diode output and doppler signal.

velocity of the particle and thus also provides the needed input for converting the measured result of block-off period to the size of the particle. However, the size of the particle so calculated can only be considered approximate due to the combined effects of the finiteness of the size of the optical measuring volume and the size of the effective scattering area of surface of the particle. For large particles of a size larger by an order-of-magnitude or more than the smaller dimension of the optical measuring volume, the error in the particle size so calculated is usually far below two percent. For small particles of a size a few times the magnitude of the smaller dimension of the optical measuring volume, these two effects seem to compensate each other to a great extent in the calculation of the size of the particle. While the relative size of the optical measuring volume becomes more pronounced for smaller particles, the size of the effective scattering area of surface of the particle becomes less extensive due to its larger curvature. The errors in the calculated particle size for such small particles, because of these effects, are found to be still as low as two percent.

3.3 Small Particle Measurement Scheme

The optical measuring volume is approximately ellipsoidal in shape with the intensity of illumination falling off from its center in the form of a three-dimensional Gaussian distribution. The particles in the flow for this scheme are assumed to be smaller than the smaller dimension of the optical measuring volume, and in the size range where the aforementioned, previously established monotonical dependence of the scattered light intensity on the particle size is held valid. It is assumed there is only one particle in the measuring volume at any given time. Then the Doppler signal amplitude becomes a function of the location of the particle path through the measuring volume and the scattering particle size as shown in sketch of Figure 7. For a usually small measuring volume (for example, 240μm in smaller dimension) and a dilute suspension (say less than $10^5/cm^3$), this assumption can be shown reasonably sound. Furthermore, such diluteness of the suspension is also required for avoiding significant attenuation of the intensity of laser beams in the two-phase mixture which is an important parameter in this scheme.

It is also assumed that the predominate direction of the flow is lined up with the measuring direction of the optical measuring system, which is the direction of the bisecting line between the axes of the incident and receiving optics at the center of the measuring volume. It is seen that the peak incident light intensity along the particle's path through the measuring volume and the length of path of the particle's center are essentially functions of the location of the path. Since the particle path length is the product of signal path time and particle velocity which is directly proportional to the signal Doppler frequency, the three useful characteristic parameters of an idealized Doppler signal, as shown in the sketch of Figure 8, are then the amplitude, Doppler frequency and path time. The assumption of the lining up of the predominate flow direction with the measuring direction of the measuring

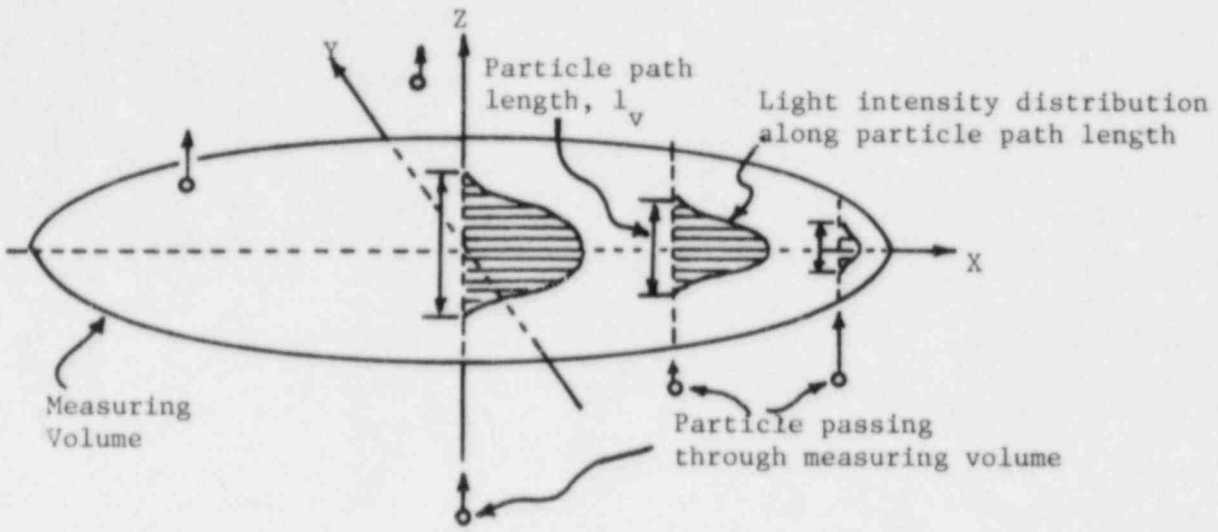

Figure 7. Sketch of optical measuring volume.

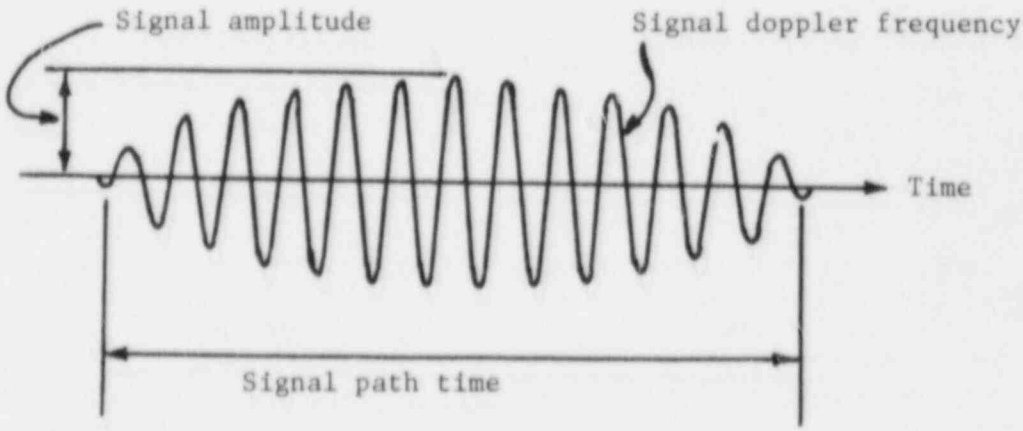

Figure 8. Sketch of particle Doppler signal.

system is not usually a severe one as it can be shown that the effect on the determination of the particle's path time would be negligibly small even if these two directions should deviate from each other by as much as 15°.

A much more serious difficulty in the determination of a particle's path time corresponding to the center of the particle through the measuring volume is the broadening of the signal. Due to the finiteness of the particle size, the raw Doppler signal is increasingly broadened in time with increase in the particle size. The following scheme has been worked out to convert the measured signal path time from a raw Doppler signal to the corrected path time corresponding to the center of the particle passing through the measuring volume for the particle size determination. By employing this scheme, the resultant calibration curve between the droplet diameter and doppler signal amplitude is shown in Figure 9 and 10.

The central portion of the amplitude of a Doppler signal, A, varies in a near Gaussian fashion while the amplitude at the two ends of the signal is broadened due to the finiteness of the size of the particle as shown in the sketch of Figure 11. Theoretically, the signal amplitude will asymptotically approach the zero amplitude base level if a truly Gaussian distribution is present. But for a fixed receiving optics, the signal amplitude reaches zero amplitude at both ends in finite time. To describe the central portion of the amplitude of the signal, a false base located at a small platform amplitude increment ΔA_b below the base of zero amplitude would have to be designated. Then, the measured path time and signal amplitude are converted by a correction scheme to an equivalent path time and an equivalent signal amplitude respectively for the same droplet as if it had passed through the center of the measuring volume. By this correction scheme, analyzed results can be statistically more stable.

3.4 Instrumentation Development and Computer Interface

A scheme making use of the various signal processors was devised for the validation of the Doppler signal. After such a validation, information on the block-off time, the velocity and the amplitude of Doppler signal for each particle was recorded. The velocity information was easily obtained from the Doppler signal frequency in digital form by using a counter signal processor (T.S.I. Model 1990). The Doppler signal amplitude was detected by first rectifying the signal using a custom-built linear rectifier, passing the rectified signal through a low-pass filter to obtain the envelope of the signal and finally using a peak detector.

The block-off time of the reference beam for the particle was obtained by using the output of the photo-diode with the proper selection of the threshold voltage level to determine the start and end of the blockage. A typical photo-diode output together with the accompanying Doppler signal on the same time scale is shown in the oscilloscope trace of Figure 6. A rectangular pulse which is proportional to the block-off time was obtained by using a high-speed amplifier and a comparator.

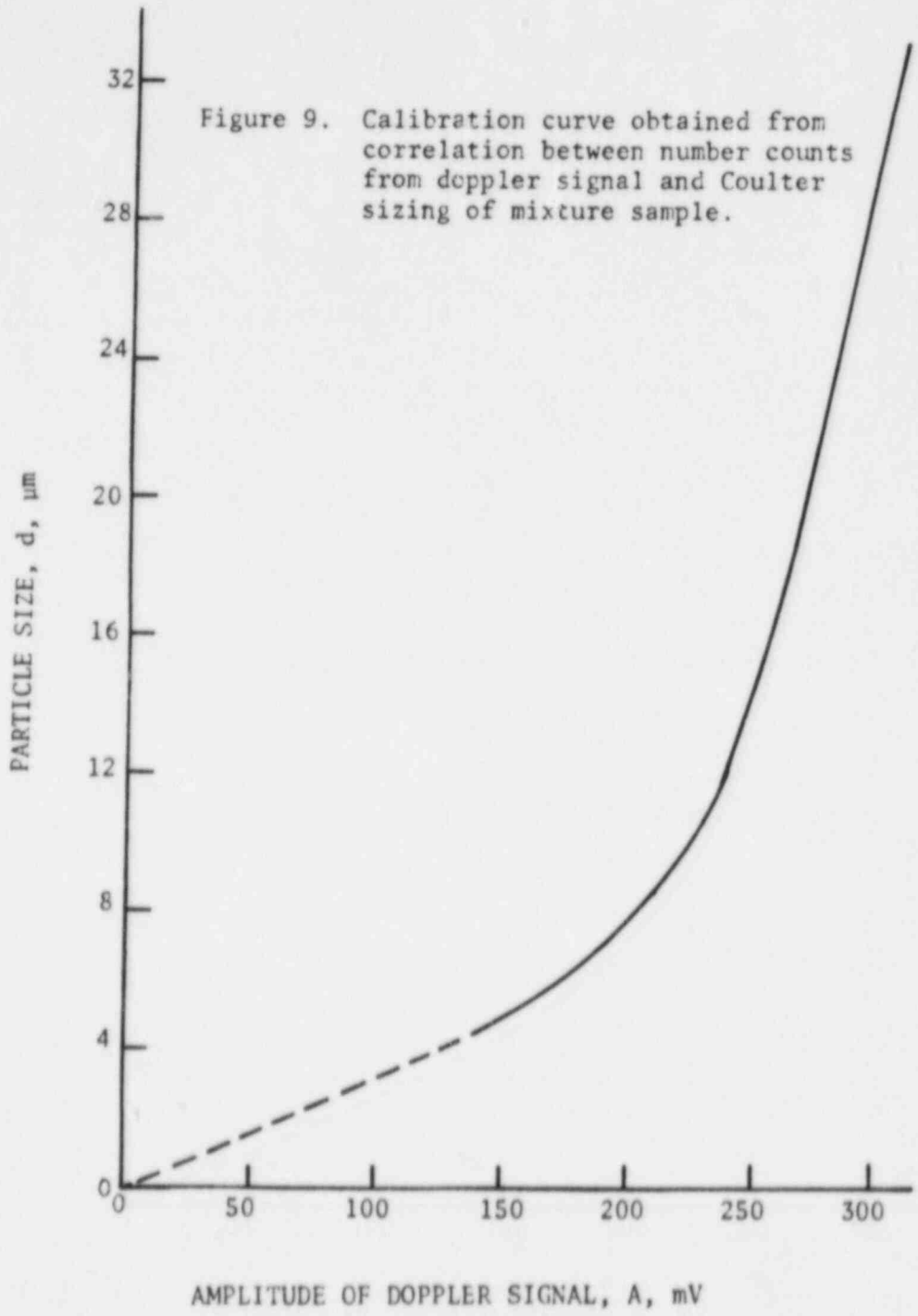

Figure 9. Calibration curve obtained from correlation between number counts from doppler signal and Coulter sizing of mixture sample.

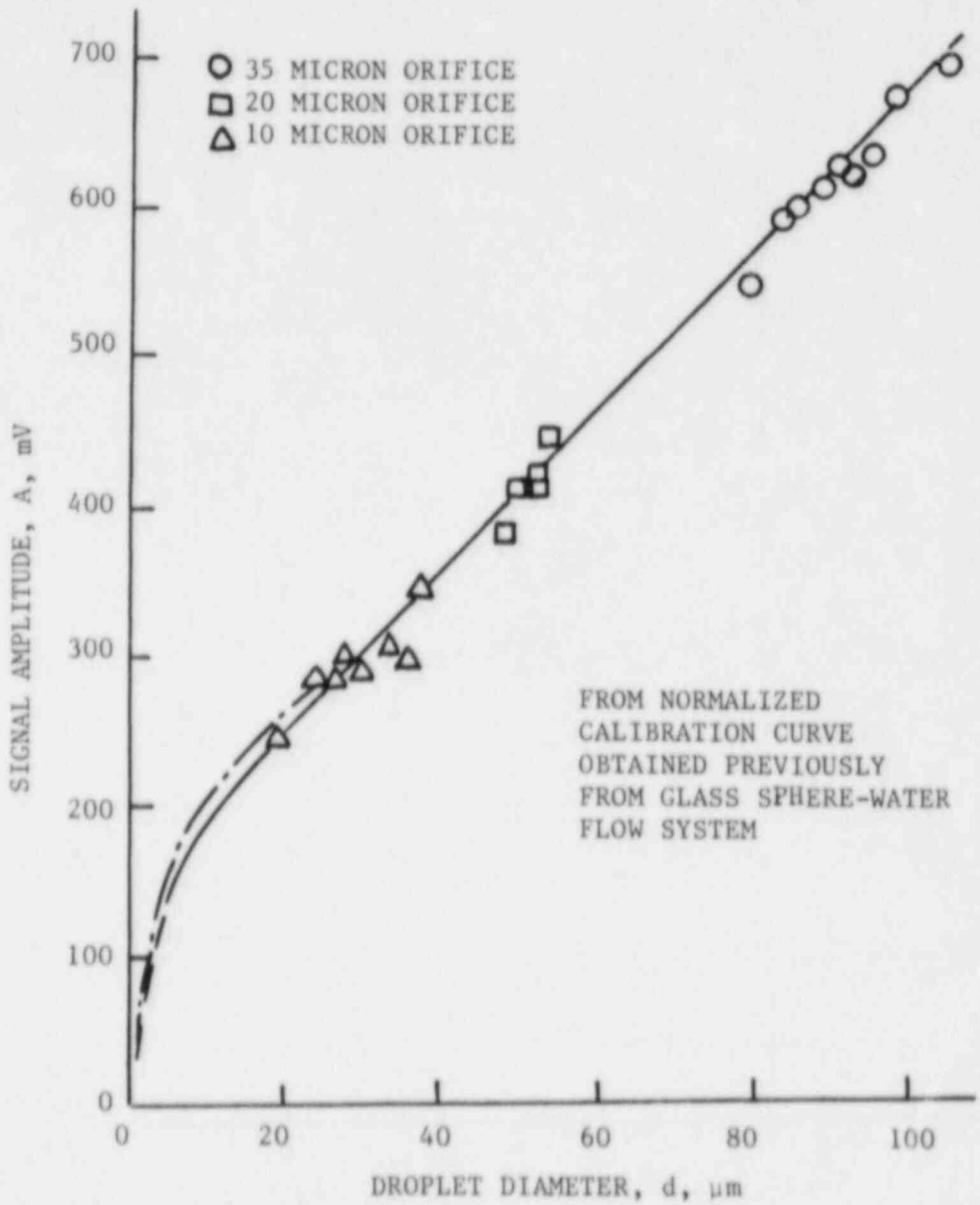

Figure 10. Calibration curve obtained from direct measurement using uniform size droplets between droplets size and doppler signal amplitude.

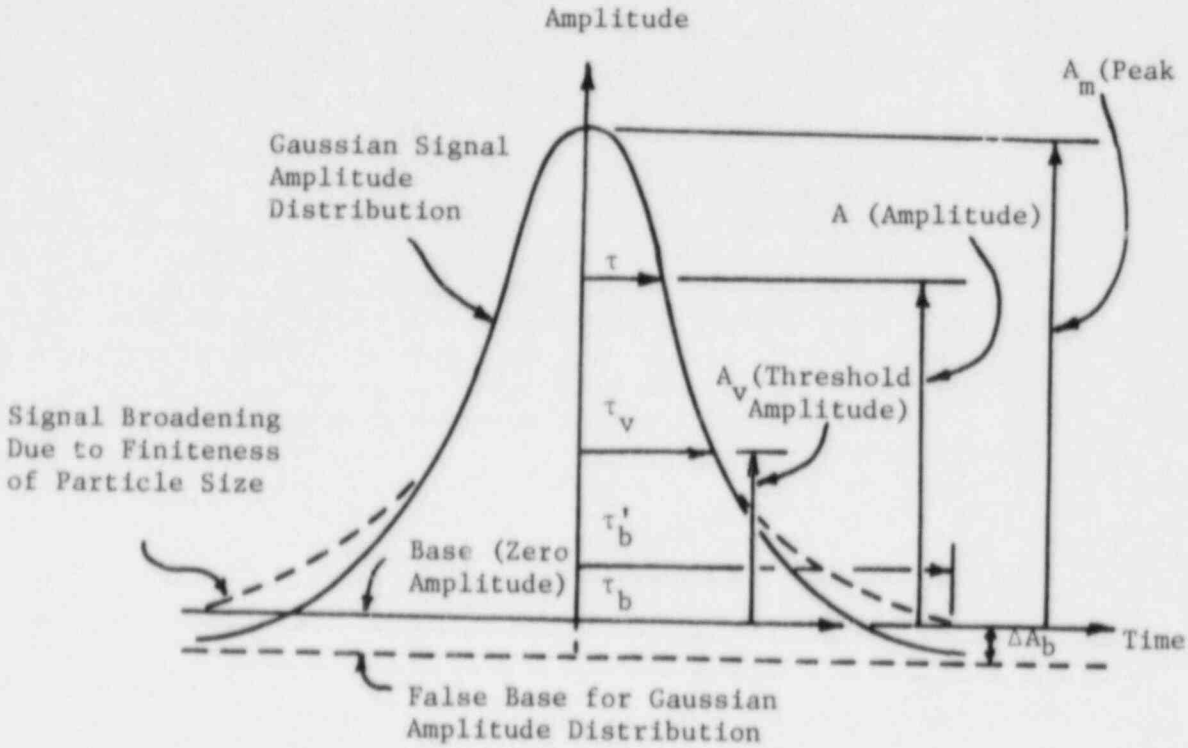

τ	Half path time at amplitude level A.
τ_v	Measured half path time at selected threshold amplitude level A_v.
τ_b'	Measured half path time for raw Doppler signal at zero amplitude (base) level.
τ_b	Corrected half path time at zero amplitude (base) level.
ΔA_b	Platform amplitude increment of base above false base for Gaussian amplitude distribution.

Figure 11. Scheme for signal path time correction for signal broadening due to finiteness of particle size.

The width of this rectangular pulse was then measured using a 5 MHz oscillator (Bailey Model TCCO-26LA) and a 20-bit digital counter using integrated circuits (74LS93). Thus, all the required parameters were obtained in the digital form.

For the storage, processing and analysis of data, a PDP-11/34 minicomputer was used. Custom-designed computer interfaces (T.S.I. Models 1998-D-1, 1998-S and 1998-Y) were used to interface the aforementioned electronic circuits to the PDP-11/34 computer interface (DR-11B). Another custom-built electronic circuit was used to validate the signals. The velocity information from the counter signal processor and the Doppler signal amplitude information from the signal peak amplitude detector circuit were latched to produce an output only when a blocking was immediately followed by a valid Doppler signal. For signals from each particle which satisfied the aforementioned validation requirements, the four pieces of digital data, vix, a) the number of cycles N selected for the validation of the Doppler signal, b) the time measured for the selected N number of cycles of the Doppler signal, c) the block-off time and d) the Doppler signal amplitude were read into the minicomputer. These data were stored in the memory of a hard disc (RK-05). The data acquisition system had been so automated that it was possible to collect as many data points as required under software control. The instrumentation block diagram for signal processing and data acquisition is illustrated in Figure 12.

4. DETAILED MEASUREMENT

All the experiments were performed at ambient atmospheric pressure and room temperature. The supplied water had a temperature of 21°C. Inside the channel, a cross-shaped nozzle assembly was located 75mm below the grid spacer. To reduce the noise-to-signal ratio in the LDA measurement, only one line of nozzle assembly was operated perpendicular to the laser beam. This line of nozzle assembly had seven nozzles and they were spaced evenly at every 4mm. The effect of grid spacer thickness was studied by employing two kinds of grid spacer thicknesses. One of them was the original thickness of 0.5mm and the other thickness was 1.17mm. The supplied water flow rate was varied from 205 cm^3/min to 535 cm^3/min. This variation corresponded to void fractions between 0.87 to 0.91. The air velocities inside the channel were varied from 11.6 m/s to 17.4 m/s.

The measurements were done at two levels above the grid spacer and one level below the grid spacer. As shown in Figure 13, the measurement Location 1 was 5mm below the grid spacer while Locations 2 and 3 were 22mm and 100mm above the grid spacer, respectively. At every level, the measurements were taken 0.9mm away from the center of the grid spacer to eliminate corner effects from a grid spacer joint. The LDA system was used to measure the size and velocity of a droplet. Two size measurement schemes were used at each measurement location. The large particle measurement scheme measured a droplet size which had a longer radius than the shorter semiaxis of the measuring volume. The small particle size measurement scheme measured a droplet size smaller

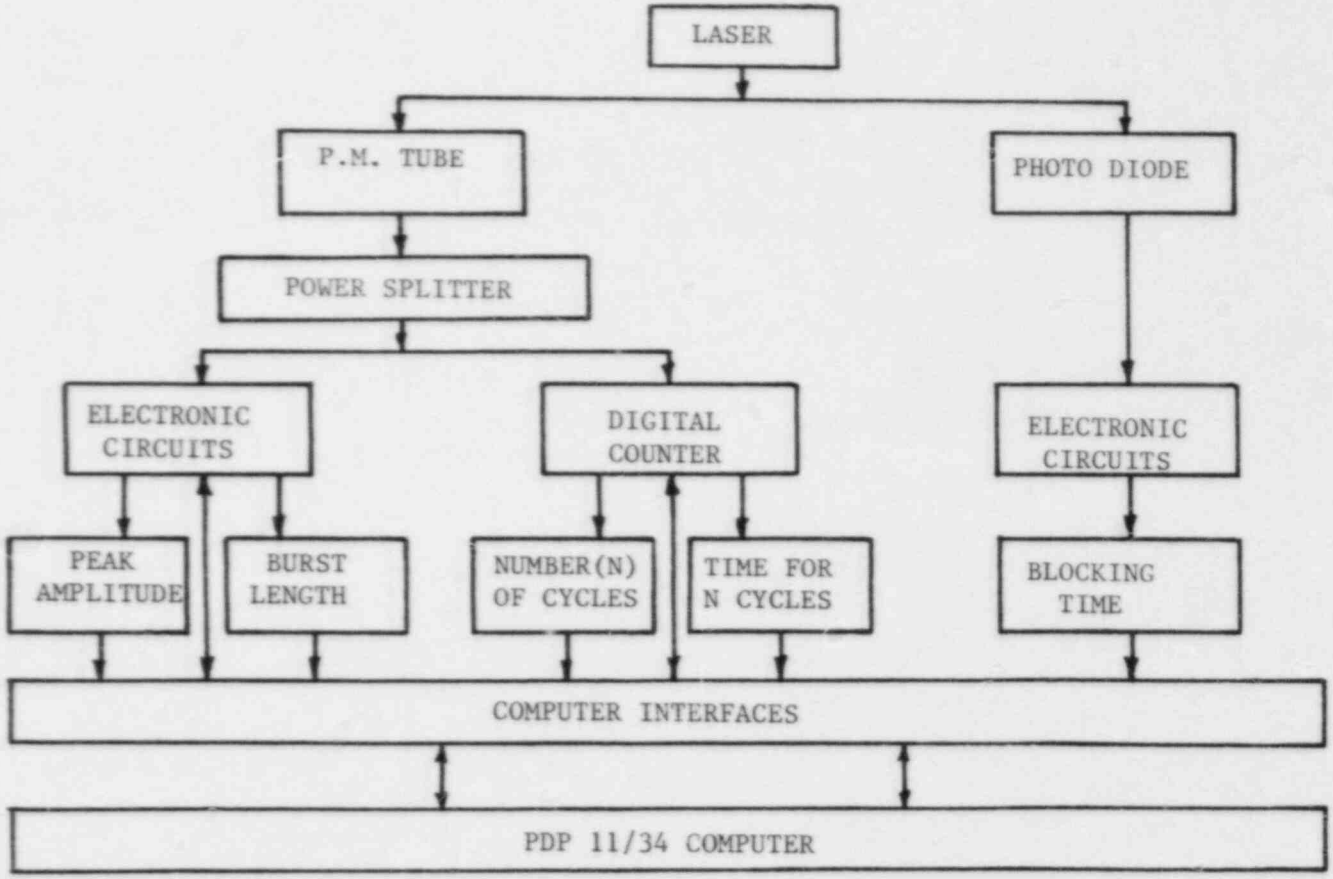

Figure 12. Instrumentation block diagram.

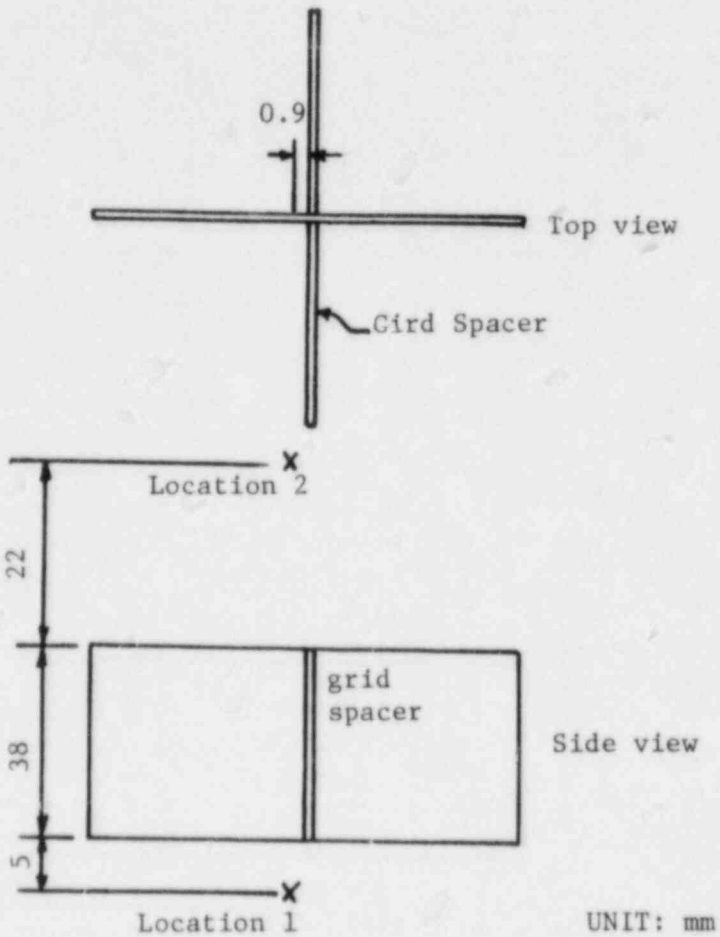

Location 1: measurement was done at 5mm below the grid spacer.

Location 2: measurement was done at 22mm above the grid spacer.

Figure 13. Measurement locations.

than the measuring volume. They are expressed by L and S, respectively. In order to keep the windows clean, compressed air was used to remove accumulated water droplets, and new windows were installed periodically. The incoming dispersion contained water droplets of sizes varying from 0.5mm to 2.5mm. However, Sauter mean diameter of reentrained small droplets showed that they were independent of other flow parameters.

All of the data were transferred to the PDP-11/34 computer direct memory board, and were analyzed to get the basic information shown in Table 1. When the large particle measurement scheme was applied, the blocking length in Table 1 represents the droplet size directly. When the small particle measurement scheme was applied, the droplet size could be obtained from the path length and signal amplitude using a calibration curve. Sample size and velocity distributions of droplets from individual signals are shown in Figures 14-21. The number densities are shown in Table 2. The Sauter mean diameters were calculated from the measured diameters by the following relation:

$$d_{sm} = \frac{\int d^3 N dd}{\int d^2 N dd} \tag{1}$$

where d_{sm}: Sauter mean diameter.

Finally all the flow conditions and measured parameters were tabulated in Tables 3 and 4 with different grid spacer thicknesses.

5. DATA ANALYSIS AND CORRELATION

The data analysis is carried out to obtain a clear understanding of the droplet's behavior across the grid spacer. The area density, which represents the ratio between the droplets' area and volume is an important parameter in a heat transfer experiment. In this analysis, a square cross sectional area, which contained four rods and two grid spacers, was considered as a region of interest, as shown in Figure 3. The actual grid spacer thickness was influenced by the incoming droplet size due to the capture of droplets by the side walls of the grid spacer. This effective grid spacer thickness was obtained from a separate experiment which gave a droplet capturing distance as shown in Figure 22. In this supplementary experiment, the water nozzle was tranversed transversely relative to the vertical grid spacer plate. For each of five initial droplet sizes, measurement was made of the grid spacer effective capture range, x, the farthest distance from the grid spacer surface at which the droplet was still captured by the surface film. The effective grid spaver thickness, ℓ, is then the sum of the actual grid spacer thickness, t, and twice this grid spacer effective capture range, $\ell = t + 2x$. The detailed area definitions are shown in Figure 3.

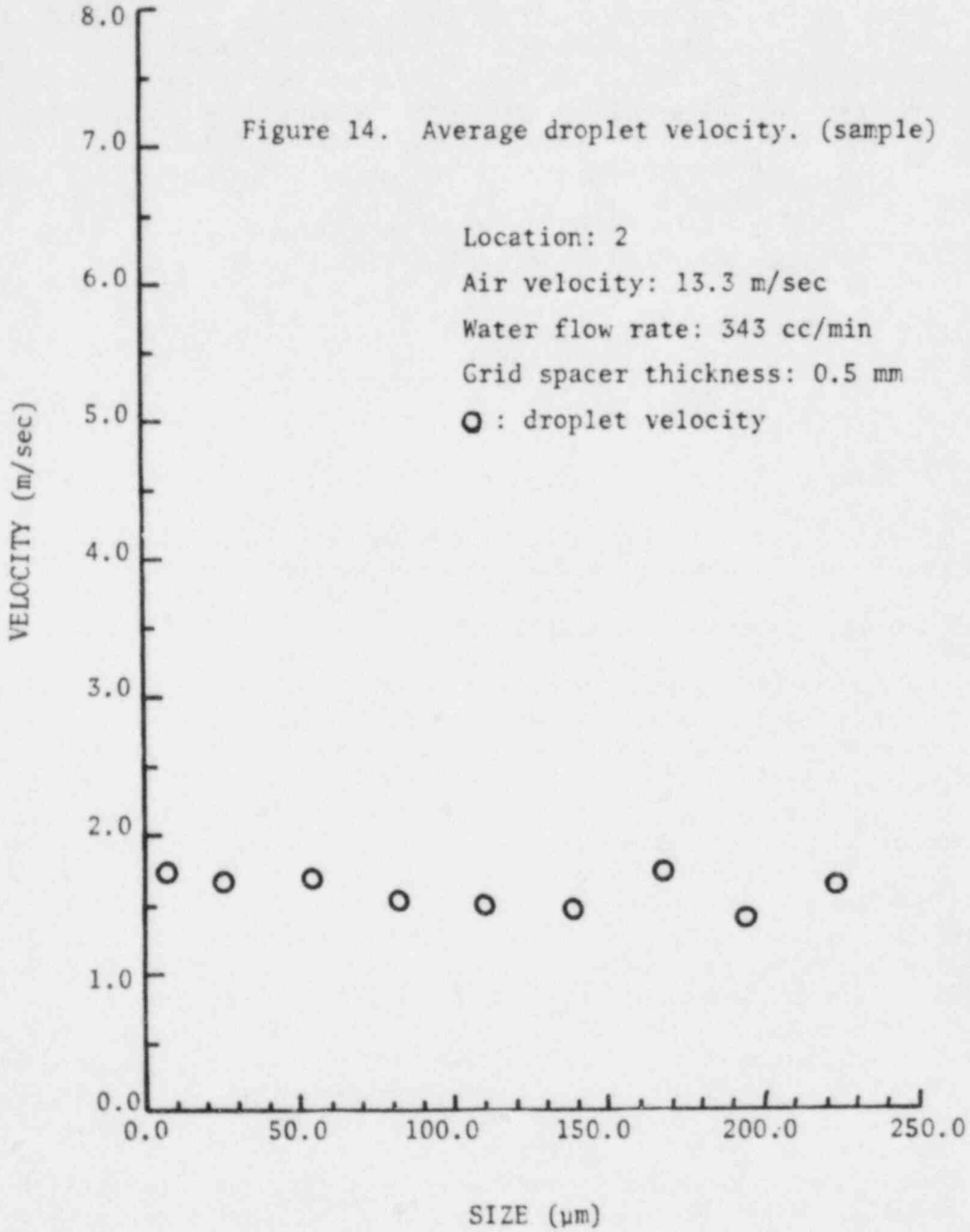

Figure 14. Average droplet velocity. (sample)

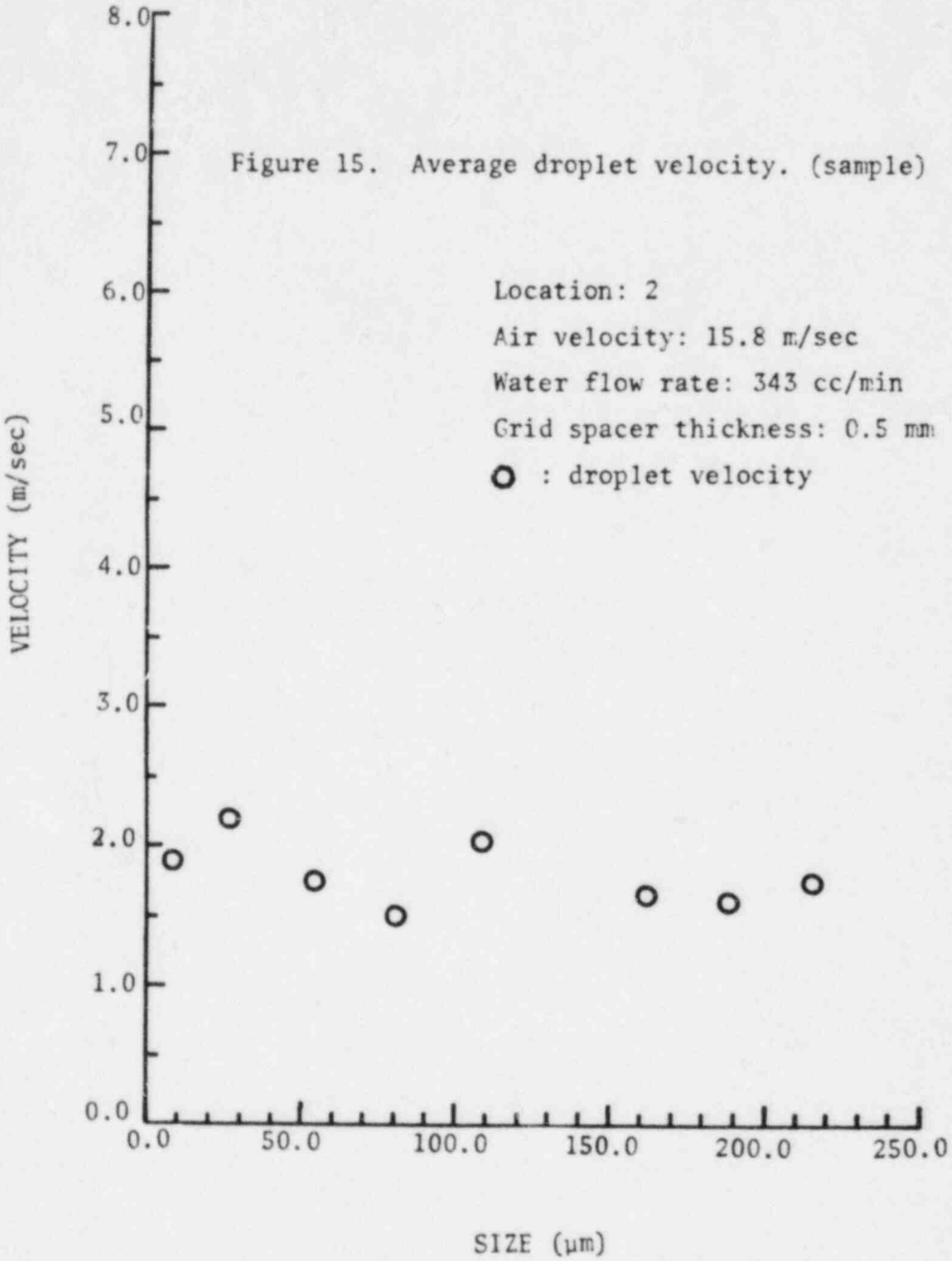

Figure 15. Average droplet velocity. (sample)

Figure 16. Size distribution.

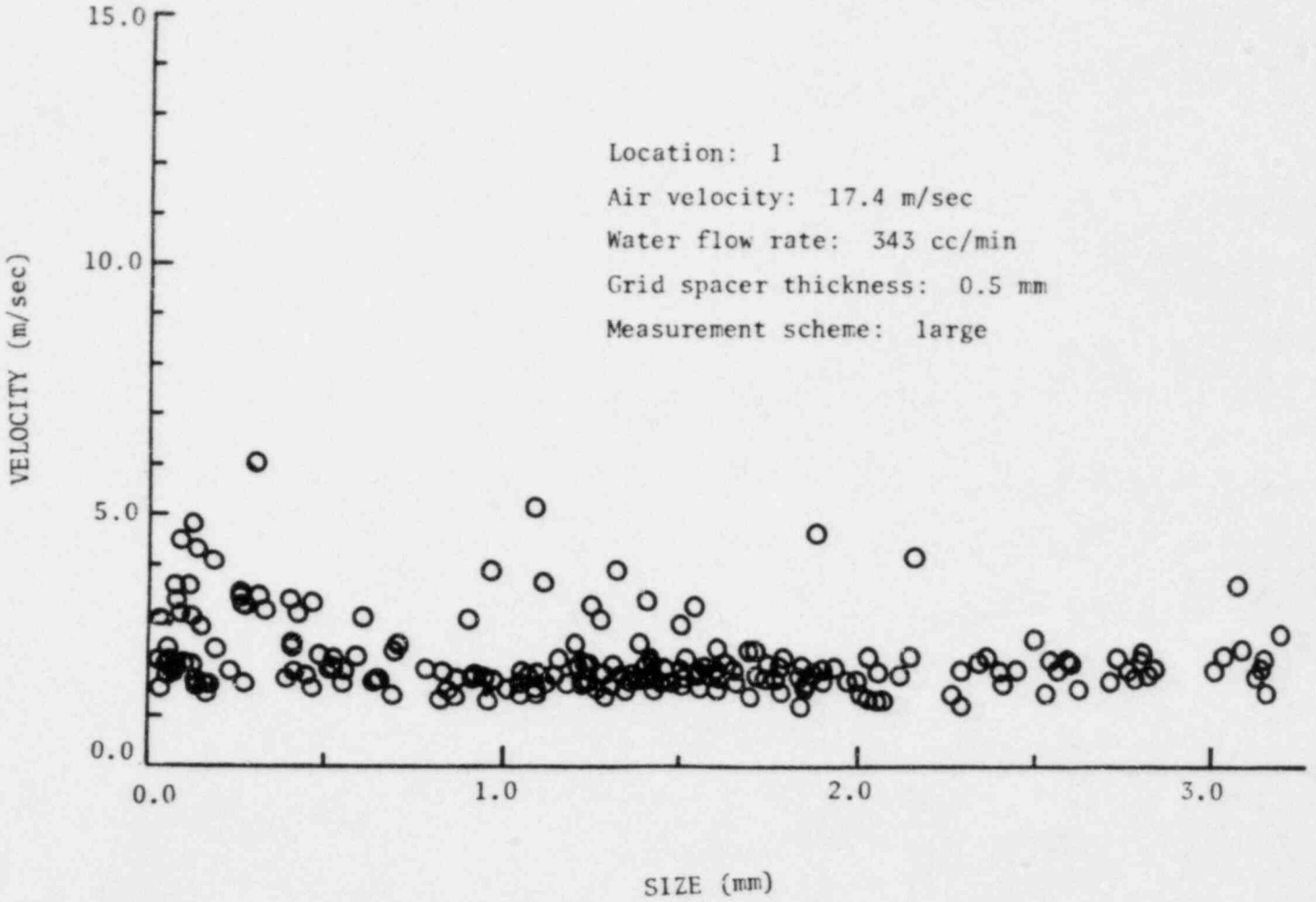

Figure 17. Size distribution.

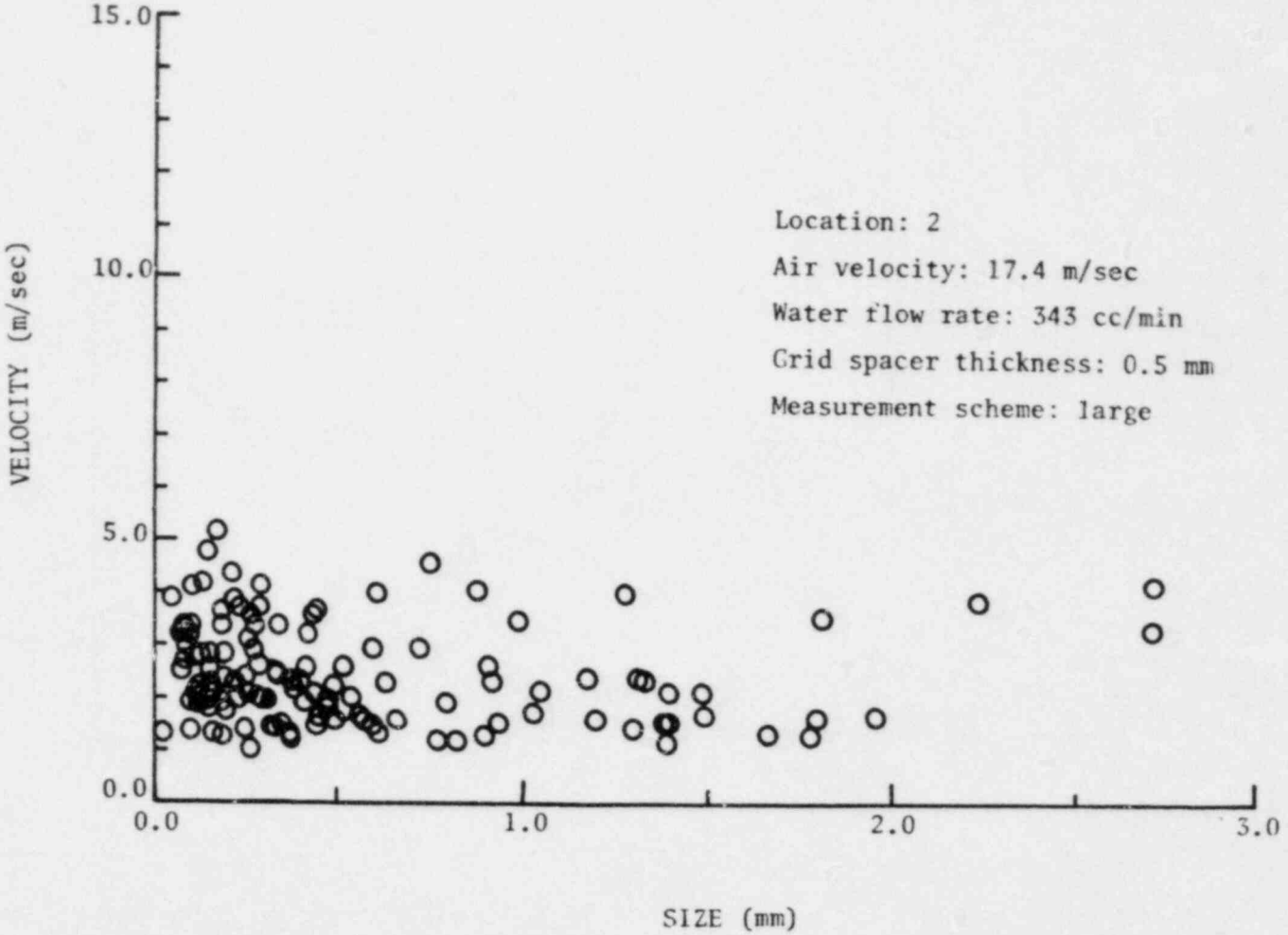

Figure 18. Size distribution.

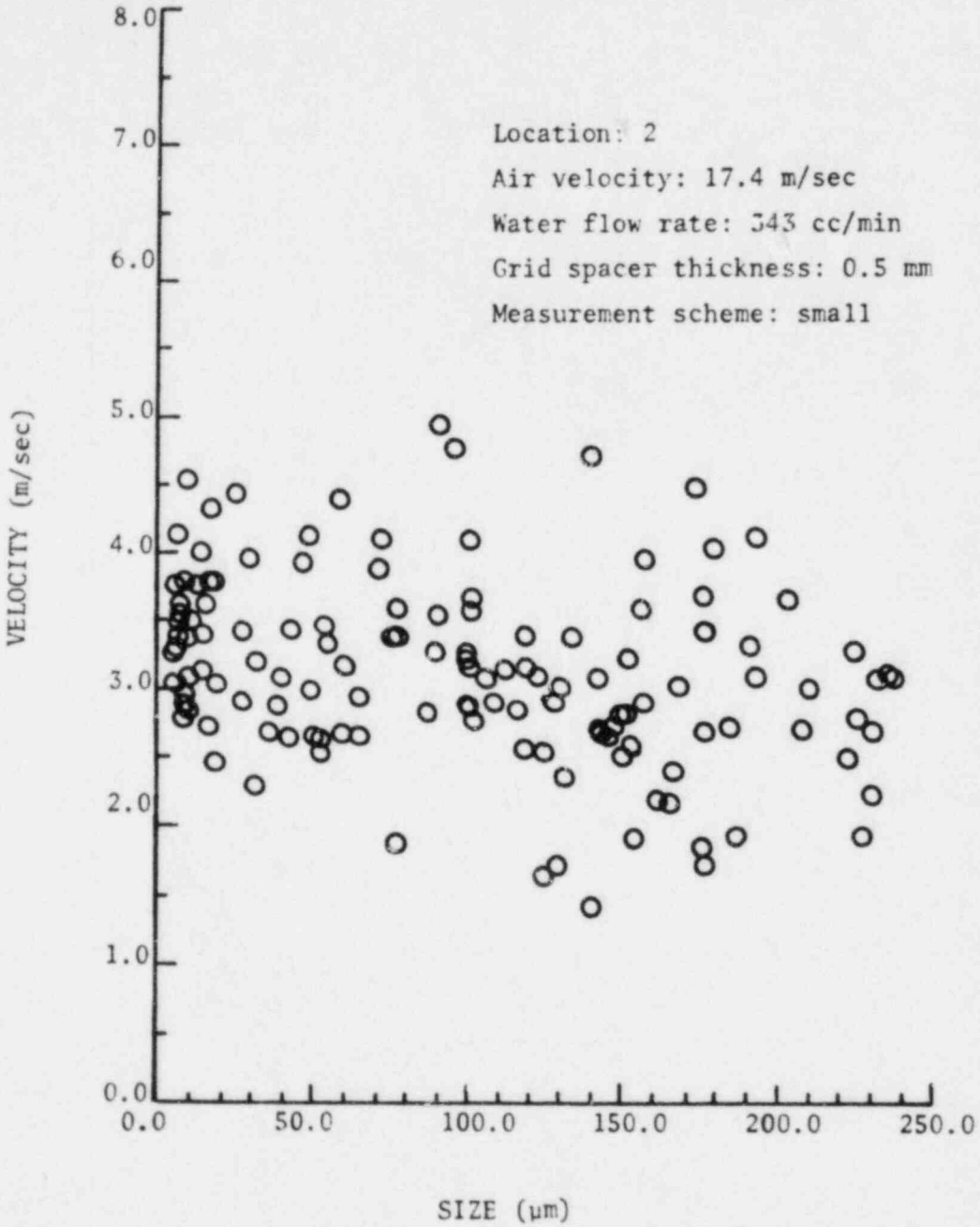

Figure 19. Size distribution.

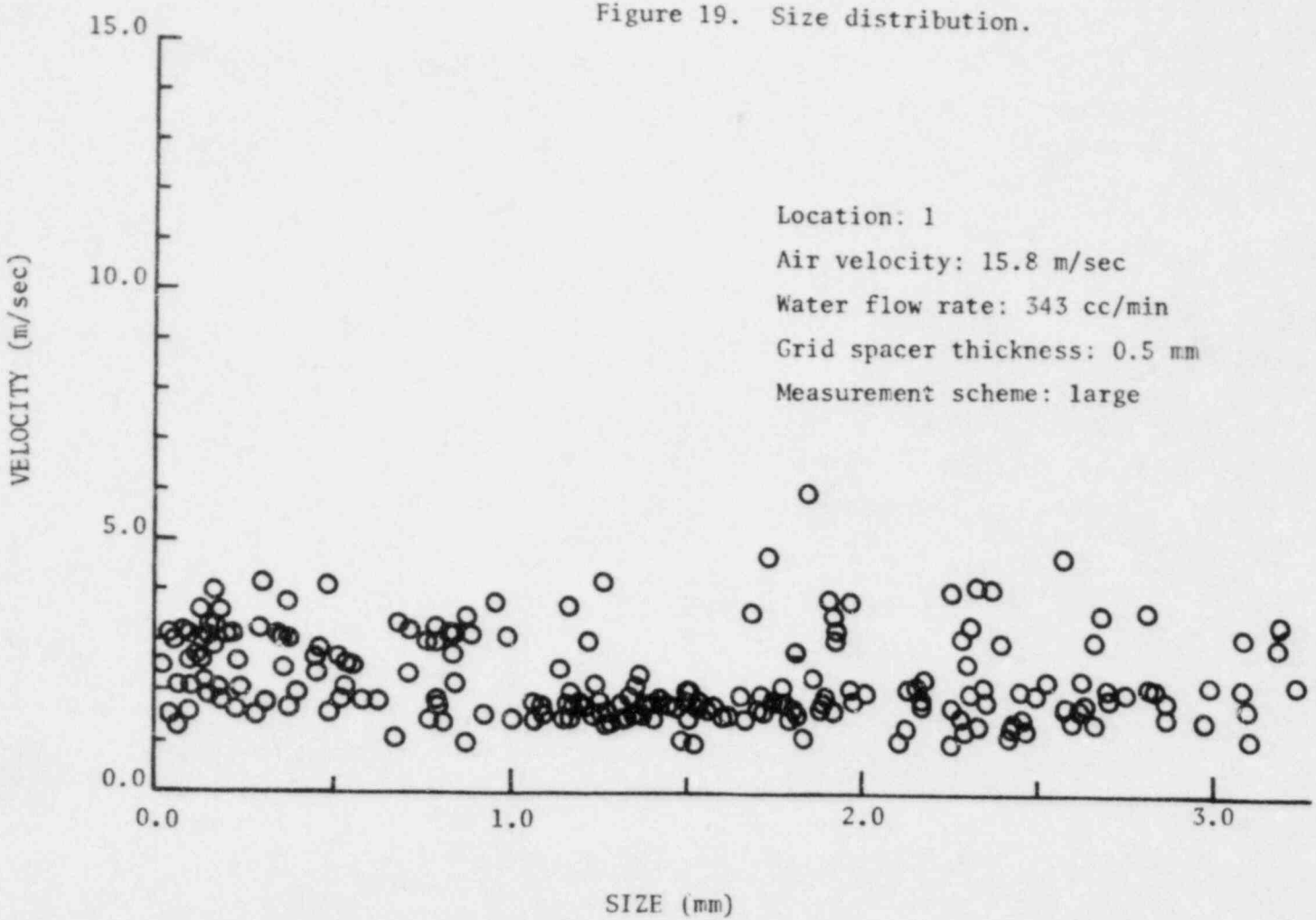

Figure 20. Size distribution.

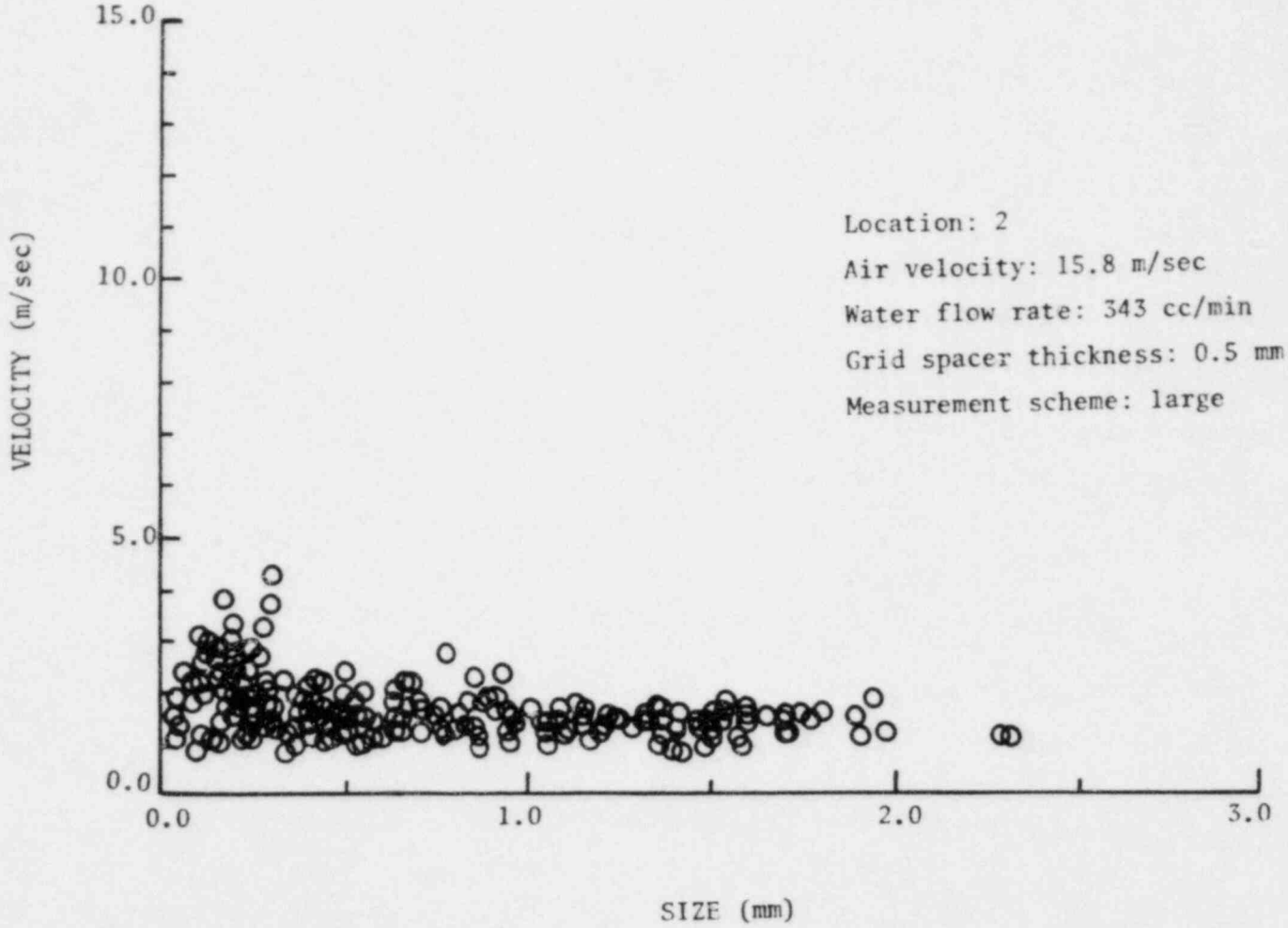

Figure 21. Size distribution.

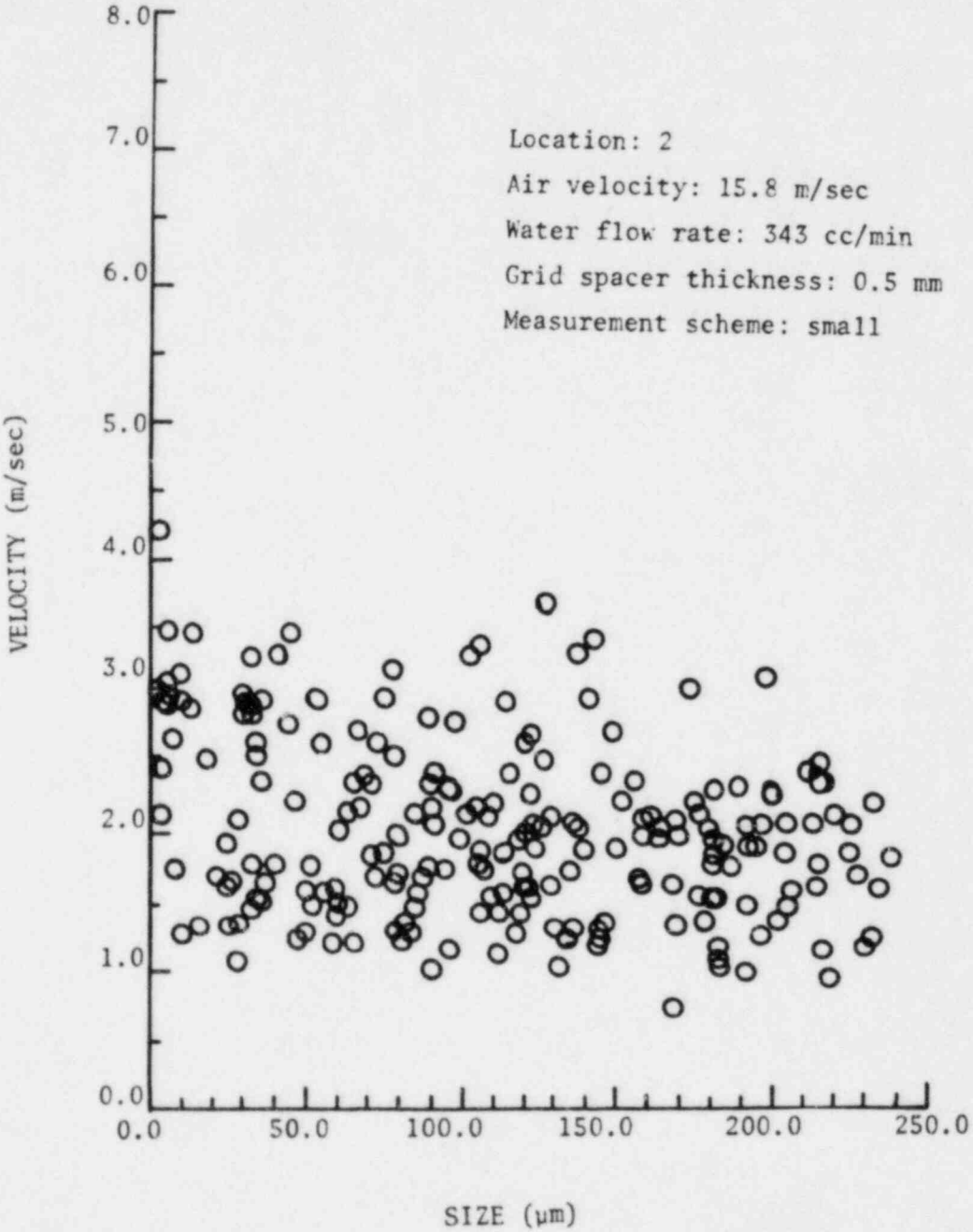

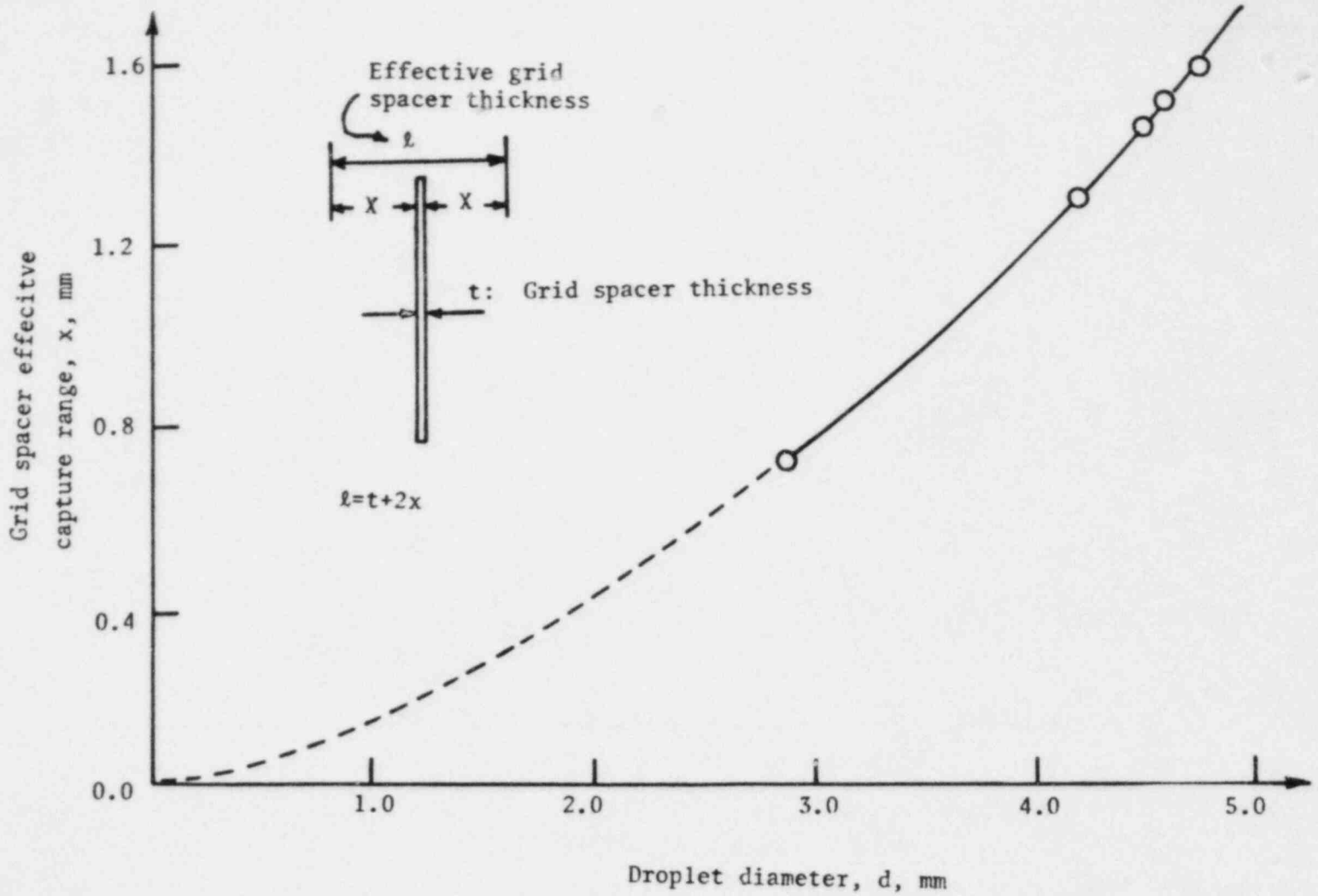

Figure 22. Measurement of effective grid spacer thickness.

TABLE 1 - SAMPLE DATA SHEET

BLOCK NUMBER: 3

AXL VEL	T BTWN SMPL	BLOCKING LEN	AMPLITUDE	PATHTIME
(M/SEC)	(MICRO SEC)	(MICROMS)	(VOLTS)	(MICROSEC)
0.17648E+01	0.25500E+06	0.59652E+02	0.17582E+00	0.33800E+02
0.14444E+01	0.25500E+06	0.18719E+03	0.42002E+00	0.12960E+03
0.38115E+01	0.25500E+06	0.20125E+03	0.39072E+00	0.52800E+02
0.17166E+01	0.25500E+06	0.56306E+02	0.20757E+00	0.32800E+02
0.39236E+01	0.25500E+06	0.31498E+04	0.18559E+00	0.80280E+03
0.19360E+01	0.25500E+06	0.17657E+03	0.10672E+01	0.91200E+02
0.29573E+01	0.25500E+06	0.10114E+03	0.17338E+00	0.34200E+02
0.31713E+01	0.25500E+06	0.83469E+03	0.13187E+00	0.26320E+03
0.20419E+01	0.25500E+06	0.91478E+02	0.24664E+00	0.44800E+02
0.12599E+01	0.25500E+06	0.81895E+02	0.47863E+00	0.65000E+02
0.25890E+01	0.25500E+06	0.58771E+03	0.14652E+00	0.22700E+03
0.83607E+00	0.25500E+06	0.13611E+03	0.81074E+00	0.16280E+03
0.27988E+01	0.25500E+06	0.11475E+03	0.28327E+00	0.41000E+02
0.28717E+01	0.25500E+06	0.63753E+02	0.12210E+00	0.22200E+02
0.18817E+01	0.25500E+06	0.19457E+03	0.33504E+01	0.10340E+03
0.11929E+01	0.25500E+06	0.13026E+03	0.72527E+00	0.10920E+03
0.17490E+01	0.25500E+06	0.10494E+03	0.23443E+00	0.60000E+02
0.20885E+01	0.25500E+06	0.12531E+03	0.64957E+00	0.60000E+02
0.16704E+01	0.25500E+06	0.28163E+03	0.84005E+00	0.16860E+03
0.21301E+01	0.25500E+06	0.84779E+02	0.21001E+00	0.39800E+02
0.11984E+01	0.25500E+06	0.14813E+03	0.21856E+01	0.12360E+03
0.14200E+01	0.25500E+06	0.20136E+03	0.65128E+01	0.14180E+03
0.18621E+01	0.25500E+06	0.14487E+03	0.47619E+00	0.77800E+02
0.34542E+01	0.25500E+06	0.18514E+03	0.12698E+00	0.53600E+02
0.30017E+01	0.19600E+06	0.46287E+03	0.11233E+00	0.15420E+03
0.91032E+00	0.25500E+06	0.66089E+02	0.28327E+00	0.72600E+02
0.13617E+01	0.25500E+06	0.70810E+02	0.34921E+00	0.52000E+02
0.20206E+01	0.19400E+06	0.94159E+02	0.21978E+00	0.46600E+02
0.19656E+01	0.45000E+05	0.10103E+03	0.28327E+00	0.51400E+02

TABLE 2

NUMBER DENSITY VS. DIAMETER (SAMPLE).

Air velocity : 17.4 m/sec.

Water flow rate: 343 cc/min.

Grid spacer thickness : 0.5 mm

Location : 22 mm above the grid spacer.

Size : Small particle measurement scheme.

MEAN DIAMETER (MICRONS)	NUMBER DENSITY (#/CC/MICRON)
224.336	0.159E+02
194.929	0.155E+02
165.522	0.181E+02
136.116	0.159E+02
106.709	0.150E+02
77.303	0.260E+02
47.896	0.236E+02
20.918	0.283E+02
4.377	0.826E+02

SUMMATION OF D**3*NUMDEN*SIZERA= 1.3216648E+10
SUMMATION OF D**2*NUMDEN*SIZERA= 7.5597192E+07

SAUTER MEAN DIAMETER(MICRON)= 174.8299

TABLE 3

FLOW CONDITIONS AND MEASURED PARAMETERS

*Grid Spacer Thickness:0.5mm (KWU)

TEST RUN NO.	WATER FLOW RATE (Q_1:cc/min)	AIR VELOCITY (Va:m/sec)	SIZE MEAS. SCHEME	MEAS. LOCATION	SAUTER MEAN DIA. (d_{sm}:μ)	DATA RATE (ω:data/sec)	DROPLET VELOCITY (Vd:m/sec)
A	343	17.4	L	1	1871.6	9.33	1.7
			S	2	174.7	1486.1	2.8
			L	2	1789.2	27.43	2.4
B	343	15.8	L	1	1972.9	8.16	1.7
			S	2	174.9	1601.0	1.8
			L	2	1563.7	19.0	1.8
C	343	13.3	L	1	1991.9	3.95	1.6
			S	2	176.9	1605.0	1.6
			L	2	1420.3	11.2	1.4
D	205	11.6	L	1	2203.7	3.72	0.8
			S	2	171.1	1560.9	1.5
			L	2	1496.7	3.14	1.2
E	535	17.4	L	1	1801.3	9.33	2.1
			S	2	158.7	1357.8	2.4
			L	2	1807.1	56.25	2.3
F	535	15.8	L	1	1853.2	8.16	2.0
			S	2	170.9	1463.4	2.1
			L	2	1708.5	43.75	2.0
G	535	13.3	L	1	1905.4	3.95	2.1
			S	2	176.2	1486.1	2.0
			L	2	1428.9	33.58	1.6

L : Measurement done by large particle measurement scheme (dia. over 240μ)

S : Measurement done by small particle measurement scheme (dia. below 240μ)

TABLE 4

FLOW CONDITIONS AND MEASURED PARAMETERS

*Grid Spacer Thickness:1.17mm
(FLECHT SEASET)

TEST RUN NO.	WATER FLOW RATE (Q_l:cc/min)	AIR VELOCITY (V_a:m/sec)	SIZE MEAS. SCHEME	MEAS. LOCATION	SAUTER MEAN DIA. (d_{sm}:μ)	DATE RATE (ω:data/sec)	DROPLET VELOCITY (Vd:m/sec
A	343	17.4	L	1	1871.6	9.33	1.7
			S	2	166.7	1485.0	2.6
			L	2	1108.0	42.46	2.3
B	343	15.8	L	1	1972.9	8.16	1.7
			S	2	170.0	1463.4	1.8
			L	2	1336.4	26.9	1.8
C	343	13.3	L	1	1991.9	3.95	1.6
			S	2	172.9	1464.4	1.4
			L	2	1318.1	18.6	1.3
D	205	11.6	L	1	2203.7	3.14	0.8
			S	2	170.3	1418.0	1.4
			L	2	1816.0	1.23	1.0
E	535	17.4	L	1	1801.3	9.33	2.1
			S	2	175.6	1486.0	2.1
			L	2	1793.0	77.6	1.9
F	535	15.8	L	1	1853.2	8.16	2.0
			S	2	178.2	1153.8	1.8
			L	2	1704.0	31.4	1.6
G	535	13.3	L	1	1905.4	25.3	2.1
			S	2	168.3	1218.2	1.6
			L	2	1580.0	9.86	1.3

$Area_{base}$: Unit base area that one nozzle can cover.

$$Area_{base} = 4 \times \ell \tag{2}$$

$Area_{sc}$: Considered total sub-channel area. (area surrounded by solid line)

$$Area_{sc} = (14)^2 - \frac{\pi}{4}(11)^2 = 100.97mm^2 \tag{3}$$

$Area_{gs}$: Effective grid spacer area where supplied large liquid droplets are captured. (area surrounded by dotted line)

$$Area_{Gs} = 2 \times 14 \times \ell - \ell^2 \tag{4}$$

$Area_{uo}$: Unblocked area where supplied large liquid droplets are passing through without hitting the grid spacer.

$$Area_{uo} = Area_{sc} - Area_{gs} \tag{5}$$

ℓ : Effective thickness of grid spacer which is the function of supplied droplet diameter.

At Location 1, void fraction can be calculated from the following relation:

$$\frac{Q_1}{7} = (1-\alpha)_1 \, A_{base} \, V_{d_1} \tag{6}$$

where Q_1 : Water supply rate through 7 nozzles to a grid spacer

α : Void fraction

A_{base} : Unit base area

V_{d_1} : Droplet velocity at Location 1.

If Q_1 and V_{d_1} are known, α can be calculated. Then the area density, which is an important parameter in the analysis of droplet evaporation in the hot gas stream, can be calculated from the following equation:

$$\frac{A_i}{V_t}_1 = \frac{6\,(1-\alpha)_1}{d_{sm_1}} \tag{7}$$

If large droplets are moving within the effective grid spacer thickness (ℓ), they might hit or scratch the grid spacer's side walls. Due to the surface tension and pressure effect, it is assumed that a liquid droplet is stretched and broken at it's neck to generate uniform size small droplets. The introduction of large droplets through Location 1 are assumed

to be broken into droplets of two size ranges at Location 2. They are large size droplets (mm range) and small size droplets (μm range).

At Location 2, the change of area density has significant meaning, because it explains the breakage of large droplets into small droplets. The fractiontal volume ratio is defined as the volume ratio of small or large droplet volume to total droplet volume.

$$\beta_{s,2} = \frac{\left[\int d^3 N dd\right]_{s,2}}{\left[\int d^3 N dd\right]_{s+L,2}} \tag{8}$$

$$\beta_{L,2} = \frac{\left[\int d^3 N dd\right]_{L,2}}{\left[\int d^3 N dd\right]_{s+L,2}} \tag{9}$$

where $\beta_{s,2}$ or $\beta_{L,2}$: Fractional volume of small or large liquid droplets with respect to the total liquid droplet volume Location 2.

The supplied water amount through Location 1 can be split into two parts which are used up for generating small and large size droplets.

$$(1-\alpha)_{s,1} = (1-\alpha)_1 \, \beta_{s,2} \tag{10}$$

$$(1-\alpha)_{L,1} = (1-\alpha)_1 \, \beta_{L,2} \tag{11}$$

where $(1-\alpha)_{s,1}$ or $(1-\alpha)_{L,1}$: Fractional amount of supplied water through Location 1 which corresponds to the volume of small or large droplets at Location 2.

The corresponding fractional area densities at Location 1 are as follows:

$$\left(\frac{A_i}{V_t}\right)_{s,1} = \beta_{s,2}\left(\frac{A_i}{V_t}\right)_1 = \beta_{s,2}\,\frac{6(1-\alpha)_1}{d_{sm_1}} \tag{12}$$

$$\left(\frac{A_i}{V_t}\right)_{L,1} = \beta_{L,2}\left(\frac{A_i}{V_t}\right)_1 = \beta_{L,2}\,\frac{6(1-\alpha)_1}{d_{sm_1}} \tag{13}$$

where: $\left(\frac{A_i}{V_t}\right)_{s,1}$ or $\left(\frac{A_i}{V_t}\right)_{L,1}$: Fractional area density at Location 1 which corresponds to the volume of small or large droplets at Location 2.

From Equations (7), (10(, (11), (12) and (13), area density ratios at Location 1 and 2 can be expressed as ratios of inverse Sauter mean diameters.

$$\frac{\left(\frac{A_i}{V_t}\right)_{s,2}}{\left(\frac{A_i}{V_t}\right)_{s,1}} = \frac{d_{sm_1}}{d_{sms,2}} \tag{14}$$

$$\frac{\left(\frac{A_i}{V_t}\right)_{L,2}}{\left(\frac{A_i}{V_t}\right)_{L,1}} = \frac{d_{sm_1}}{d_{smL,2}} \tag{15}$$

where $\frac{\left(\frac{A_i}{V_t}\right)_{s,2}}{\left(\frac{A_i}{V_t}\right)_{s,1}}$ or $\frac{\left(\frac{A_i}{V_t}\right)_{L,2}}{\left(\frac{A_i}{V_t}\right)_{L,1}}$: Ratios of area densities for the small or large droplets between Location 1 and Location 2.

Since d_{sm_1}, $d_{smL,2}$, $d_{sms,2}$, $\left(\frac{A_i}{V_t}\right)_{s,1}$, $\left(\frac{A_i}{V_t}\right)_{L,1}$ are already known, then area densities for large and small droplets at Location 2 can be calculated. The small droplet's area density ratio at Location 2 was increased by about 10 times, while the large droplet's area density ratio at Location 2 was increased by only 1.5 times. Hence, after liquid droplet breakage, the droplet's surface area is increased a great deal thereby serving to enhance the evaporation cooling mechanism. The related specific interfacial area flux for small droplets, $\left(\frac{A_i}{V_t}\right)_{s,2} \cdot V_{dL,1}$, or large droplets $\left(\frac{A_i}{V_t}\right)_{L,2} \cdot V_{dL,1}$ at Location 2 are also calculated.

So far, the region of interest is only restricted to the area of effective grid spacer. If all the subchannel area is considered, the area density ratios before and after grid spacer through the whole subchannel will be as follows:

$$\left(\frac{A_i}{V_t}\right)_{AGS} = \left(\frac{A_i}{V_t}\right)_{BGS}\left(\frac{Area_{uo}}{Area_{sc}}\right) + \left(\frac{A_i}{V_t}\right)_2\left(\frac{Area_{gs}}{Area_{sc}}\right)$$

$$\left(\frac{A_i}{V_t}\right)_{AGS} \quad \left(\frac{A_i}{V_t}\right)_{BGS} = \left(\frac{Area_{uo}}{Area_{sc}}\right) + \frac{\left(\frac{A_i}{V_t}\right)_2}{\left(\frac{A_i}{V_t}\right)_1}\left(\frac{Area_{gs}}{Area_{sc}}\right) \qquad (16)$$

Results of the above calculation are tabulated in Tables 5 and 6 for each of the two grid spacer thicknesses used, respectively.

After the trends of all data have been carefully analyzed, those data were correlated in several ways. All the correlations below are given in non-dimensionalized form and are shown in Figures 23-26.

1) Sauter mean diameter of the large droplets at Location 2 can be correlated with V_a and h.

$$\frac{d_{smL,2}}{d_{smL,1}} = 0.162\ (We)^{0.75}\left(\frac{h}{d_{smL,1}}\right)^{0.062} \qquad (17)$$

Uncertainty: ±9.73%
(APPENDIX A)

where $d_{smL,2}$: Sauter mean diameter of large liquid droplets which were measured at Location 2.

$d_{smL,1}$: Sauter mean diameter of large liquid droplets which were measured at Location 1.

We : $\frac{\rho_a V_a^2 d_{smL,1}}{\sigma}$ (Weber No.)

ρ_a : Supplied air density

V_a : Supplied air velocity

σ : Surface tension

h : Height of grid spacer plate.

A possible explanation of the phenomena described by the correlation is as follows:

Water droplets, after hitting the grid spacer, slide along the grid spacer as discontinous lumps because of the driving force of the supplied air. At high air velocities, the effect of air driving force is much greater than that of the surface tension. Consequently, the droplets may momentarily contact the water film on the grid spacer and then be drawn back into the channel flow. Hence, the droplet size remains nearly the same in size as when it first hits the grid spacer. However, when the air velocity is reduced, the time that the droplets spent on the grid spacer becomes longer. Small droplets are then generated from the

TABLE 5

DATA ANALYSIS

*Grid Spacer Thickness: 0.5mm (KWU)

TEST RUN NO.		d_{sml} (μ)	$(1-\alpha)_1$	$\left(\frac{Ai}{Vt}\right)_1$ (M^{-1})	$d_{sms,2}$ $d_{smL,2}$ (μ)	$\beta_{s,2}$ or $\beta_{L,2}$	$(1-\alpha)_{s,1}$ or $(1-\alpha)_{L,1}$	$\left(\frac{Ai}{Vt}\right)_{s,2} / \left(\frac{Ai}{Vt}\right)_{s,1}$ or $\left(\frac{Ai}{Vt}\right)_{L,2} / \left(\frac{Ai}{Vt}\right)_{L,1}$	$\left(\frac{Ai}{Vt}\right)_{s,2}$ or $\left(\frac{Ai}{Vt}\right)_{L,2}$ (M^{-1})	$\left(\frac{Ai}{Vt}\right)_{s,2} \cdot V_{d_{L,1}}$ or $\left(\frac{Ai}{Vt}\right)_{L,2} \cdot V_{d_{L,1}}$ (M/M-sec)	$Area_{GS}$ (MM^2)	$\frac{\left(\frac{Ai}{Vt}\right)_{AGS}}{\left(\frac{Ai}{Vt}\right)_{BGS}}$
A	S,2	1871.6	0.102	326.99	174.7	0.2132	0.0218	10.71	746.78	1269.5	31.65	4.302
	L,2				1789.2	0.7868	0.0803	1.05	269.11	457.08		
B	S,2	1972.9	0.0969	294.69	174.9	0.4091	0.0396	11.28	1360.14	2312.0	33.18	4.483
	L,2				1563.7	0.5909	0.0573	1.26	219.70	373.5		
C	S,2	1991.9	0.1013	305.14	176.9	0.4595	0.0466	11.26	1578.79	2526.0	33.69	4.858
	L,2				1420.3	0.5405	0.0548	1.40	231.30	370.1		
D	S,2	2203.7	0.1074	292.42	171.1	0.8354	0.0897	12.88	3145.72	2516.0	37.74	5.702
	L,2				1496.7	0.1646	0.0177	1.47	70.87	56.0		
E	S,2	1801.3	0.1263	421.0	158.7	0.0206	0.0026	11.34	98.44	206.7	32.16	4.467
	L,2				1807.1	0.9794	0.1237	0.96	396.86	833.4		
F	S,2	1853.2	0.1294	419.0	170.9	0.0397	0.0051	10.82	177.09	371.9	32.16	4.472
	L,2				1709.5	0.9603	0.1243	1.08	435.08	914.9		
G	S,2	1905.4	0.1326	418.78	176.2	0.112	0.0149	10.78	505.71	1062.0	32.16	4.539
	L,2				1428.9	0.888	0.1178	1.33	495.78	991.57		

TABLE 6

DATA ANALYSIS

*Grid Spacer Thickness: 0.5mm
(FLECHT SEASET)

TEST RUN NO.	d_{sml} (μ)	$(1-\alpha)_1$	$\left(\frac{Ai}{Vt}\right)_1$ (M^{-1})	$d_{sms,2}$ $d_{smL,2}$ (μ)	$\beta_{s,2}$ or $\beta_{L,2}$	$(1-\alpha)_{s,1}$ or $(1-\alpha)_{L,1}$	$\left(\frac{Ai}{Vt}\right)_{s,2}/\left(\frac{Ai}{Vt}\right)_{s,1}$ or $\left(\frac{Ai}{Vt}\right)_{L,2}/\left(\frac{Ai}{Vt}\right)_{L,1}$	$\left(\frac{Ai}{Vt}\right)_{s,2}$ or $\left(\frac{Ai}{Vt}\right)_{L,2}$ (M^{-1})	$\left(\frac{Ai}{Vt}\right)_{s,2} \cdot V_{d_{L,1}}$ or $\left(\frac{Ai}{Vt}\right)_{L,2} \cdot V_{d_{L,1}}$ (M/M-sec)	$Area_{GS}$ (MM^2)	$\frac{\left(\frac{Ai}{Vt}\right)_{AGS}}{\left(\frac{Ai}{Vt}\right)_{BGS}}$
A $\frac{S,2}{L,2}$	1871.6	0.0651	208.8	166.7	0.1592	0.0104	11.22	372.97	634.0	48.38	6.705
				1108.0*	0.840	0.0547	1.69	296.11	503.0		
B $\frac{S,2}{L,2}$	1972.9	0.0659	191.3	170.0	0.3359	0.0416	11.61	745.7	1268.0	49.83	6.972
				1336.4	0.6641	0.0213	1.48	187.5	318.8		
C $\frac{S,2}{L,2}$	1991.9	0.0661	199.1	172.9	0.5851	0.0387	11.52	1342.0	2147.0	50.32	6.996
				1318.1	0.4149	0.0274	1.51	124.8	199.7		
D $\frac{S,2}{L,2}$	2203.3	0.073	198.8	169.2	0.9594	0.0462	13.02	1624.4	1301.0	54.5	8.433
				1201.0	0.1406	0.0268	1.84	88.6	70.9		
E $\frac{S,2}{L,2}$	1801.3	0.0810	259.8	175.6	0.0255	0.0021	10.65	70.5	148.1	48.86	6.174
				1793.0	0.9745	0.0789	1.04	264.1	554.7		
F $\frac{S,2}{L,2}$	1853.2	0.0792	240.9	178.2	0.07	0.0014	11.07	186.6	391.9	48.86	6.435
				1704.0	0.9297	0.0778	1.16	259.3	544.0		
G $\frac{S,2}{L,2}$	1905.4	0.0851	256.3	168.8	0.2149	0.0183	11.80	650.0	1365.0	48.86	6.837
				1580.0	0.7851	0.0668	1.26	253.7	538.0		

* The result is not reliable due to unsteady conditions.

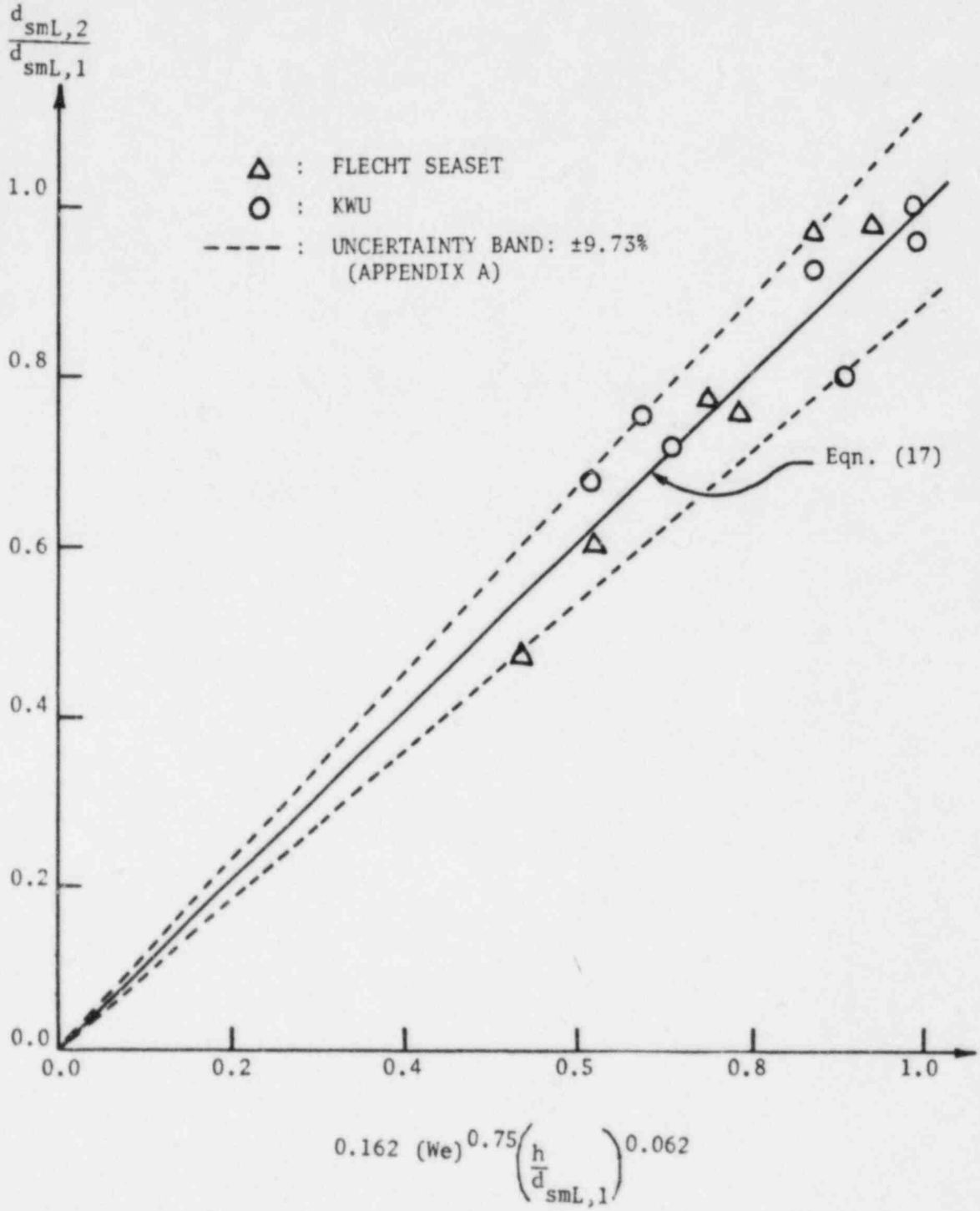

Figure 23. Sauter mean diameter of large droplets after grid spacer.

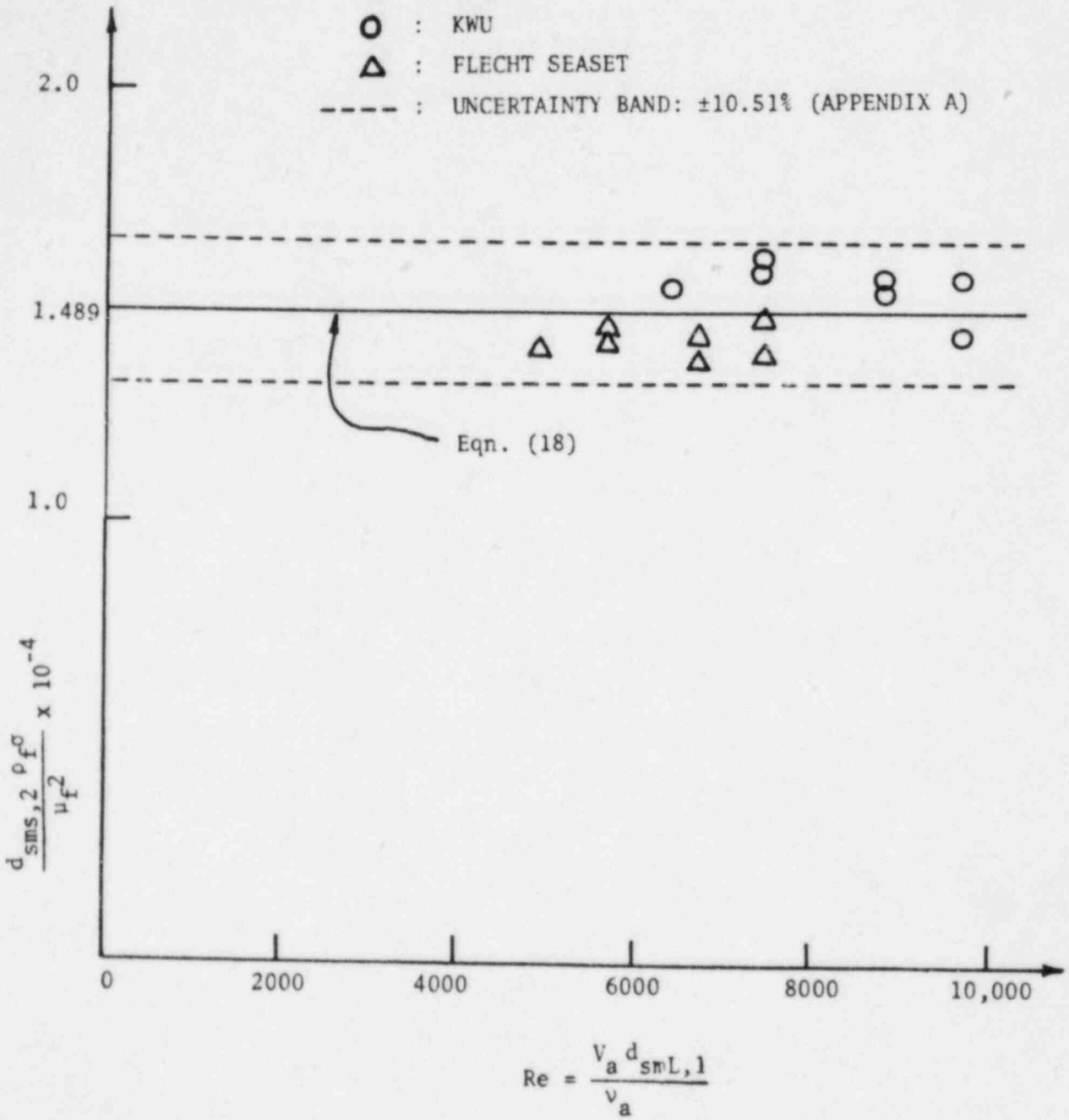

Figure 24. Sauter mean diameter of small droplets after grid spacer.

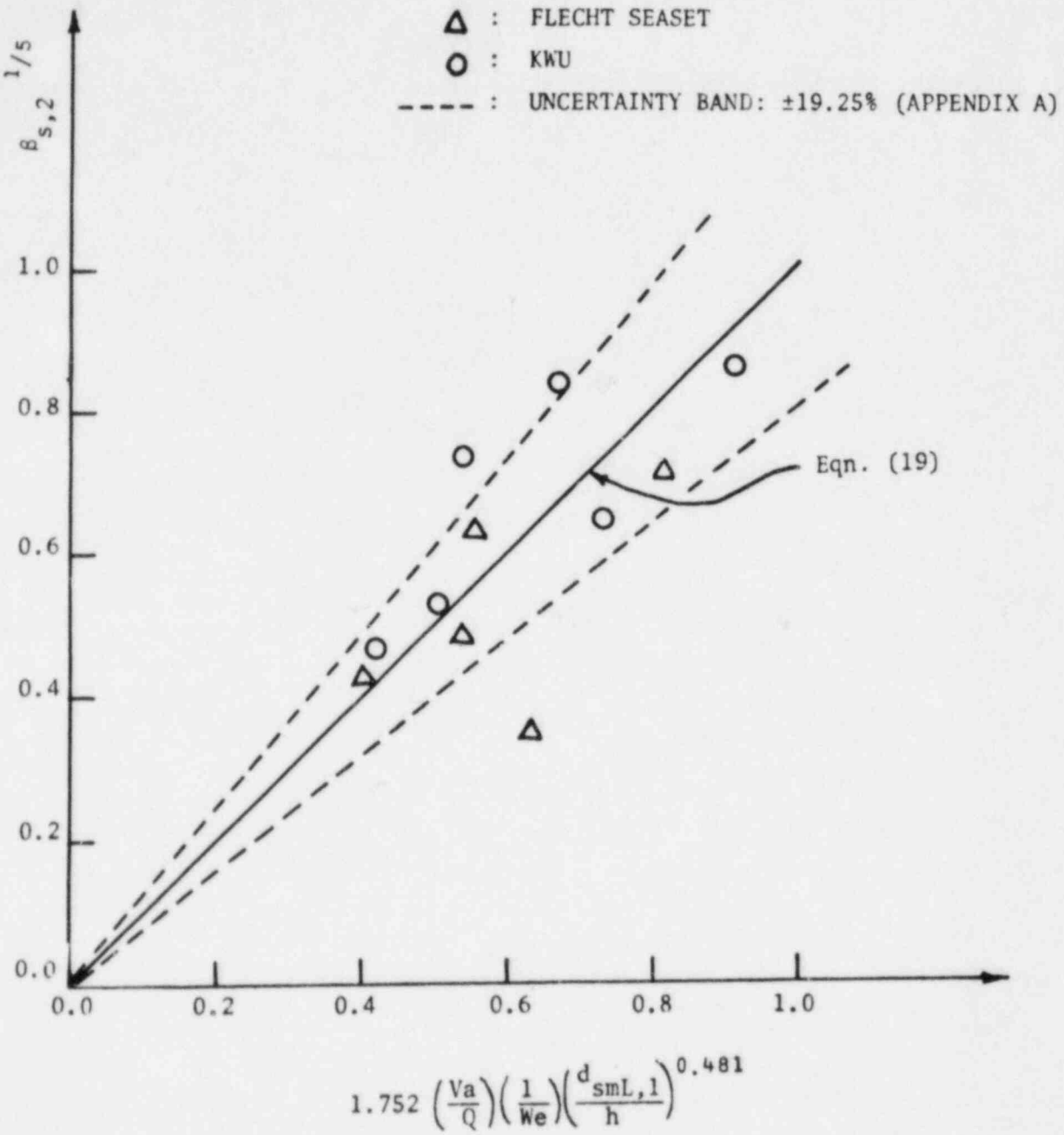

Figure 25. Fractional volume of small droplets after grid spacer.

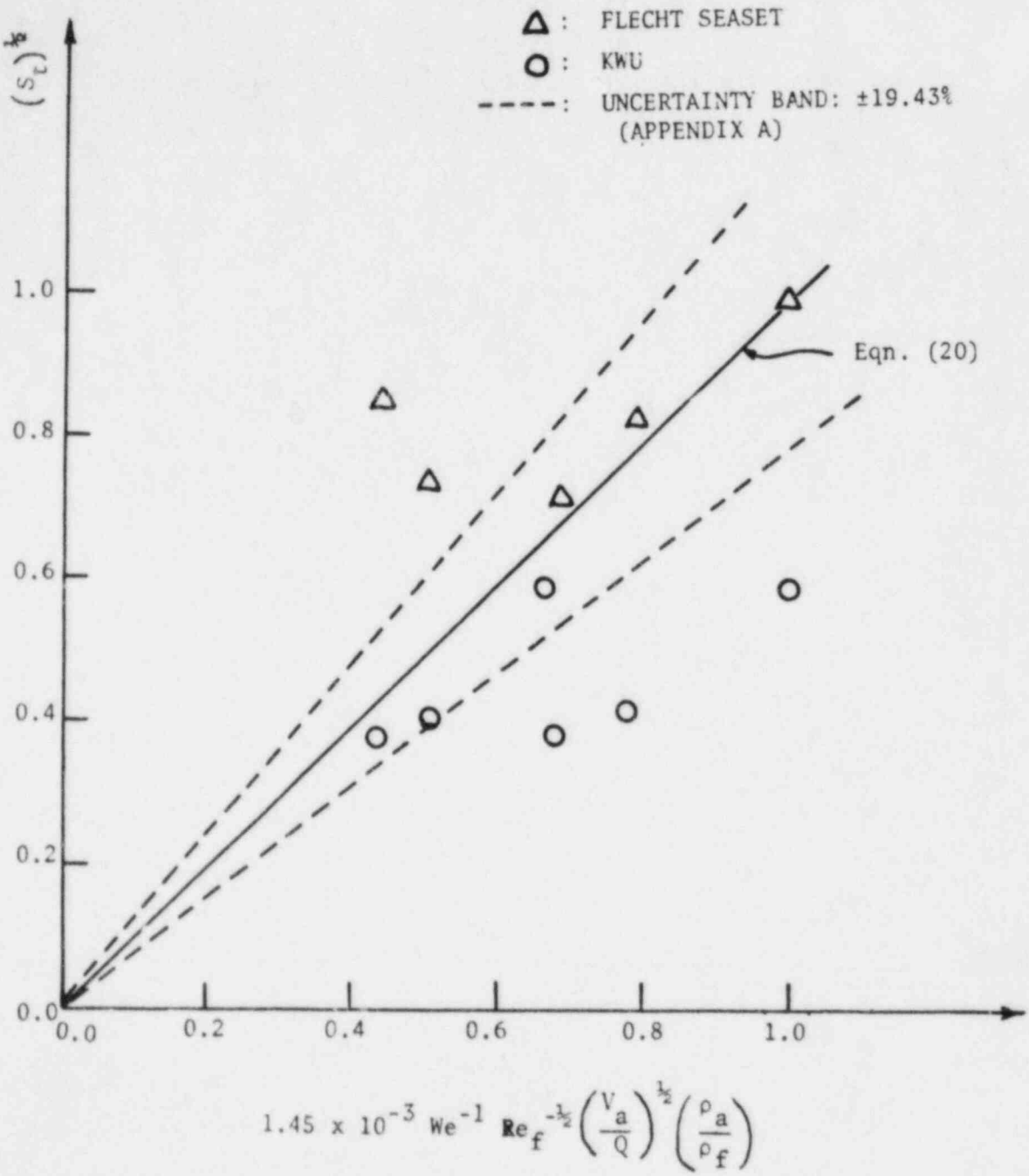

Figure 26. Nozzle characteristic.

breaking up of the trailing edge created by film entrainment mechanism. For this reason, under similar water supply, lower air velocities generate smaller droplets than higher air velocities.

2) Sauter mean diameter of the small droplets at Location 2 is uniform.

$$d_{sms,2} = 1.489 \times 10^{4} \cdot \frac{\mu_f^2}{\rho_f \sigma} \qquad (18)$$

Uncertainty: ±10.51%
(APPENDIX A)

3) Fractional volume of small droplets at Location 2 can be correlated with Q and V_a

$$\left(\beta_{s,2}\right)^{1/5} = 1.752\left(\frac{V_a}{Q}\right)\left(\frac{1}{We}\right)\left(\frac{d_{smL,1}}{h}\right)^{0.481} \qquad (19)$$

Uncertainty: ±19.25%
(APPENDIX A)

$\left(\beta_{s,2}\right)$: Fractional volume of the small liquid droplets with respect to the total liquid droplets volume at Location 2.

4) The following correlation represents nozzle characteristics:

$$\left(S_t\right)^{\frac{1}{2}} = 1.45\times10^{-3}\ We^{-1}\ Re_f^{-\frac{1}{2}}\left(\frac{V_a}{Q}\right)^{\frac{1}{2}}\left(\frac{\rho_a}{\rho_f}\right) \qquad (20)$$

Uncertainty: ±19.43%
(APPENDIX A)

S_t : $\dfrac{\nu_f}{\omega\, d_N^2}$ (Stokes No.)

ν_f : Kinematic viscosity of fluid (water)

ω : Droplet generation frequency at Location 1.

d_N : Nozzle diameter

We : $\dfrac{\rho_a V_a^2 d_N}{\sigma}$ (Weber No.)

Re_f : $\dfrac{d_N\, Q\, \rho_f}{\mu_f}$ (fluid Reynold's No.)

Q : Water supply rate through nozzles per unit grid spacer area.

μ_f : Dynamic viscosity of fluid.

The above correlation gives a relation between droplets generation frequency at Location 1 with V_a and Q.

A brief analysis of the accuracy of the optical measurement scheme is given in APPENDIX B.

REFERENCES

1. "ECCS Evaluation Models," Code of Federal REgulations 10, Part 50, Appendix K, pp.438, January 1, 1982.

2. Ihle, P., Rust, K. and Lee, S. L., "Mist Core Cooling During the Reflood Phase of PWR-LOCA," Proceedings of the International Meeting on Thermal Nuclear Reactor Safety, American Nuclear Society, Chicago, Ill., August 29 - September 2, 1982, in print.

3. Tong, L. S. and Bennet, G. L., "NRC Water-Reactor Safety-Research Program," Nuclear Safety, Vol. 18, No. 1, pp.1-40, January - February, 1977.

4. Era, A. et al., "Heat Transfer Data in the Liquid Deficient Region for Stream-Water Mixtures at 70 kg/cm^2 Flowing in Tubular and Annular Conduits," Italian Report, CISE-R-184, June 1966.

5. Ihle, P. and Rust, K., "FEBA (Flooding Experiments with Blocked Arrays) - Influence of Blockage Shape," ENR, Hamburg, May 6-11, 1979.

6. Meyer, L. C., "Treatment of Measurement Uncertainties at the Power Burst Facility," Review Group Conference on Advanced Instrumentation for Reactor Safety Research, July 29-31, 1980, Oak Ridge, Tenn.

7. Private communication with L. E. Hochreiter, Westinghouse Electric Corporation.

APPENDIX A - ERROR ANALYSIS

A variety of methods have been used to perform uncertainty analysis, each probably being optimum for some particular situation or application. The method used here is based on the model proposed at the U.S. NRC Review Group Conference by Meyer [6]. This uncertainty analysis methodology is derived from the NBS Model. It is simple and easily understood. This following section is as reproduced from the Reference [6] and applied to our measurements.

All measurements have errors which are the difference between the measurement and the true value. The maximum error that might reasonably be expected is called uncertainty. This has two components; a fixed error which is called bias, and a random error which is called precision. The bias, B, is the constant or systematic error. Each measurement has the same bias in repeated measurements and the bias cannot be determined unless the measurements are compared with true value of the quantity measured.

The random error, S, is the variation between repeated measurements. It is a measure of standard deviation. The statistic, S, is calculated to estimate the standard deviation and is called the precision index.

$$S = \sqrt{\frac{\sum_{i=1}^{N} (X_i - \bar{X})^2}{N-1}}$$

where X_i = i^{th} measurement
$\bar{X}$ = arithmetic mean
N = number of measurements.

The basic error sources fall into three categories which are:
(a) calibration errors, (b) data acquisition errors, and (c) data reduction errors.

Calibration errors contribute the most to the total uncertainty. Data acquisition errors are usually small compared with the data acquisition errors. Data reduction errors are usually much smaller. The method used to calculate the uncertainty for our measurements is based on the conceptual design as shown in Figure A.1 [6].

$$B_{Meas} = \pm \sqrt{B_{cal}^2 + B_{\substack{Data \\ Acq}}^2 + B_{\substack{Data \\ Red}}^2}$$

(A) $$B_{Cal}^2 = b_{Electronics}^2 + b_{Interface}^2 + b_{Counter}^2$$

$$= 0.2^2 + 1.0^2 + 0.1^2$$

$$B_{Cal} = 1.025\%$$

(B) $B^2_{\text{Data Acq}} = b^2_{\text{Electronics}} + b^2_{\text{Computer Interface}}$

$= 0.5^2 + 0.25^2$

$B_{\text{Data Acq}} = 0.559\%$

Hence $B_{\text{Meas}} = \pm \sqrt{1.025^2 + 0.559^2}$

$= 1.168\%$

In our experiments this random error is estimated for different parameters and are shown below. The maximum random error is used to report the uncertainty number.

Reporting Uncertainty:

The uncertainty parameter, U, is calculated using the following relationship:

$$U_{\text{Meas}} = \pm B_{\text{Meas}} + 2 \times S_{\text{Meas}}$$

The random error, S_{Meas}, for each parameter is as follows:

Description	S_{Meas}		Reading Value		S_{Meas}(%)
Air density (ρ_a)	4×10^{-3}	kg/m^3	1.197	kg/m^3	0.33
Liquid density (ρ_f)	0.2	kg/m^3	998.2	kg/m^3	0.02
Air velocity (V_a)	0.03	m/sec	15.5	m/sec	0.19
Droplet velocity (V_{dl})	0.05	m/sec	2.53	m/sec	1.98
Sauter mean diameter of large liquid droplet $(d_{smL,1})$	71.4	µm	1641.7	µm	4.35
Nozzle diameter (d_N)	0.015	mm	0.8	mm	1.88
Height of grid spacer(h)	0.1	mm	38.0	mm	0.26
Water flow rate (Q)	4.46	cc/min	343	cc/min	1.30
Surface tension (σ)	0.2	dyne/cm	73.6	dyne/cm	0.27
Liquid dynamic viscosity (u_f)	0.022	cp	1.005	cp	2.19
Unit base area (A_{base})	0.03	mm^2	5.2	mm^2	0.58

*All values are based on the room temperature of 20°C.

*S_{Meas} (%) = $\frac{S_{\text{Meas}}}{\text{Reading Value}} \times 100$

The random errors S_{Meas} of the correlations can be obtained from the differential form of correlations.

1) The correlation of Sauter mean diameter of large droplets at Location 2 is

$$\frac{d_{smL,2}}{d_{smL,1}} = 0.162\,(We)^{0.75}\left(\frac{h}{d_{smL,1}}\right)^{0.062}$$

The random error of this correlation is

$$S_{\left(\frac{d_{smL,2}}{d_{smL,1}}\right)} = \frac{\partial\left(\frac{d_{smL,2}}{d_{smL,1}}\right)}{\partial(We)} S_{(We)} + \frac{\partial\left(\frac{d_{smL,2}}{d_{smL,1}}\right)}{\partial\left(\frac{h}{d_{smL,1}}\right)} S_{\left(\frac{h}{d_{smL,1}}\right)}$$

Then the percentile random error can be expressed as follows:

$$\frac{S_{\left(\frac{d_{smL,2}}{d_{smL,1}}\right)}}{\left(\frac{d_{smL,2}}{d_{smL,1}}\right)} \times 100 = \left[0.75\,\frac{S_{(We)}}{We} + 0.062\left(\frac{S_{(h)}}{h} + \frac{S_{d_{smL,1}}}{d_{smL,1}}\right)\right] \times 100$$

$$= \left[0.75\left(\frac{S_{(\rho_a)}}{\rho_a} + 2\cdot\frac{S_{(V_a)}}{V_a} + \frac{S_{(d_{smL,1})}}{d_{smL,1}} + \frac{S_{(\sigma)}}{\sigma}\right) + 0.062\left(\frac{S_{(h)}}{h} + \frac{S_{(d_{smL,1})}}{d_{smL,1}}\right)\right] \times 100$$

$$= \left[0.75 \times (0.33 + 2\times 0.19 + 4.35 + 0.27) + 0.062\,(0.26 + 4.35)\right]$$

$$= 4.28\%$$

where: $We = \frac{\rho_a V_a^2 d_{smL,1}}{\sigma}$

$$\frac{S_{(We)}}{We} = \frac{S_{(\rho_a)}}{\rho_a} + 2\cdot\frac{S_{(V_a)}}{V_a} + \frac{S_{(d_{smL,1})}}{d_{smL,1}} + \frac{S_{(\sigma)}}{\sigma}$$

Therefore, uncertainty of this correlation is

$$U_{\left(\frac{d_{smL,2}}{d_{smL,1}}\right)} = \pm\,(1.168 + 2\times 4.28) = \pm\,9.73\%$$

2) The correlation of Sauter mean diameter of the small droplets at Location 2 is

$$d_{sms,2} = 1.489 \times 10^{4} \cdot \frac{\mu_f^2}{\rho_f \sigma}$$

The percentile random error of this correlation is

$$\frac{S_{(d_{sms,2})}}{d_{sms,2}} \times 100 = \left(2 \times \frac{S_{(\mu_f)}}{\mu_f} + \frac{S_{(\rho_f)}}{\rho_f} + \frac{S_{(\sigma)}}{\sigma} \right) \times 100$$

$$= (2 \times 2.19 + 0.02 + 0.27)$$

$$= 4.67$$

Then the uncertainty of this correlation is

$$U_{d_{sms,2}} = \pm (1.168 + 2 \times 4.67) = \pm 10.51\%$$

3) The correlation of fractional volume of small droplets at Location 2 is

$$\left(\beta_{S,2}\right)^{1/5} = 1.752 \left(\frac{V_a}{Q}\right)\left(\frac{1}{We}\right)\left(\frac{d_{smL,1}}{h}\right)^{0.481}$$

The percentile random error of this correlation can be expressed as

$$\frac{S_{(\beta_{S,2})^{1/5}}}{(\beta_{S,2})^{1/5}} \times 100 = \left[\left(\frac{S_{(V_a)}}{V_a} + \frac{S_{(Q)}}{Q} \right) + \left(\frac{S_{(\rho_a)}}{\rho_a} + 2 \cdot \frac{S_{(V_a)}}{V_a} + \frac{S_{(d_{smL,1})}}{d_{smL,1}} + \frac{S_{(\sigma)}}{\sigma} \right) + 0.481 \times \left(\frac{S_{(d_{smL,1})}}{d_{smL,1}} + \frac{S_{(h)}}{h} \right) \right] \times 100$$

$$= \left[(0.19 + 1.30) + (0.33 + 2 \times 0.19 + 4.35 + 0.27) + 0.481 \, (4.35 + 0.26) \right]$$

$$= 9.04\%$$

Therefore uncertainty of this correlation is

$$U_{(\beta_{S,2})^{1/5}} = \pm (1.168 + 2 \times 9.04) = \pm 19.25\%$$

4) The correlation of the nozzle characteristic is

$$\left(S_t\right)^{1/2} = 1.45\times10^{-3}\ (We)^{-1}\left(Re_f\right)^{-1/2}\left(\frac{V_a}{Q}\right)^{1/2}\left(\frac{\rho_a}{\rho_f}\right)$$

The percentile random error of this correlation is

$$\frac{S\left(S_t\right)^{1/2}}{\left(S_t\right)^{1/2}} \times 100 = \left[\left(\frac{S\left(\rho_a\right)}{\rho_a} + 2\times\frac{S\left(V_a\right)}{V_a} + \frac{S\left(d_{smL,1}\right)}{d_{smL,1}} + \frac{S(\sigma)}{\sigma}\right) + \frac{1}{2}\left(\frac{S\left(d_N\right)}{d_N} + \frac{S_{(Q)}}{Q} + \frac{S\left(\rho_f\right)}{\rho_f} + \frac{S\left(\mu_f\right)}{\mu_f} + \frac{1}{2}\left(\frac{S\left(V_a\right)}{V_a} + \frac{S_{(Q)}}{Q}\right) + \left(\frac{S\left(\rho_a\right)}{\rho_a} + \frac{S\left(\rho_f\right)}{\rho_f}\right)\right)\right] \times 100$$

$$= \left[(0.33 + 2\times0.19 + 4.35 + 0.27) + \frac{1}{2}\,(1.88 + 1.3 + 0.02 + 2.19) + \frac{1}{2}\,(0.19 + 1.30) + (0.33 + 0.02)\right]$$

$$= 9.13\%$$

Where: $$\frac{S\left(Re_f\right)}{Re_f} = \frac{S\left(d_N\right)}{d_N} + \frac{S_{(Q)}}{Q} + \frac{S\left(\rho_f\right)}{\rho_f} + \frac{S\left(\mu_f\right)}{\mu_f}$$

Therefore, uncertainty of this correlation is

$$U\left(S_t\right)^{1/2} = \pm\ (1.168 + 2\times9.13) = \pm\ 19.43\%$$

5) The area density is given by Equations (6) and (7).

$$\left(\frac{A_i}{V_t}\right)_1 = \frac{6(1-\alpha)_1}{d_{sm,1}} = \frac{6}{7}\ \frac{Q_1}{d_{sm,1}\,A_{base}\,V_{d_1}}$$

The percentile random error of this equation is

$$\frac{S\left(\frac{A_i}{V_t}\right)_1}{\left(\frac{A_i}{V_t}\right)_1} \times 100 = \left[\frac{S_{(Q)}}{Q} + \frac{S\left(d_{smL,1}\right)}{d_{smL,1}} + \frac{S\left(A_{base}\right)}{A_{base}} + \frac{S\left(V_{d_1}\right)}{V_{d_1}}\right] \times 100$$

$$= (1.30 + 4.35 + 0.58 + 1.98)$$

$$= 8.21\%$$

$$= (1.30 + 4.35 + 0.58 + 1.98)$$

$$= 8.21\%$$

So, the uncertainty of the area density is

$$U_{\left(\frac{A_i}{V_t}\right)_1} = \pm (1.168 + 2x8.21) = \pm 17.59\%$$

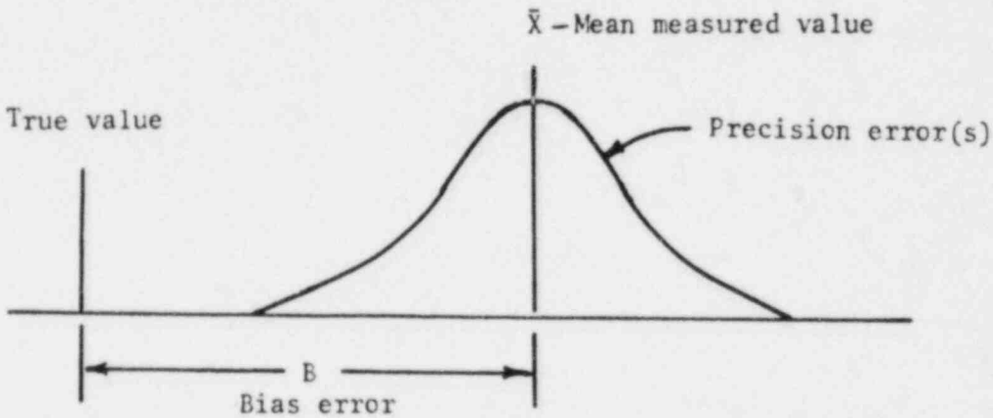

FIGURE A.1. MEASUREMENT ERROR.

APPENDIX B - ACCURACY OF THE MEASUREMENT SCHEME

The following is an analysis of the error introduced if the flow direction deviates from the measuring direction by a small angle α, where α is in radians.

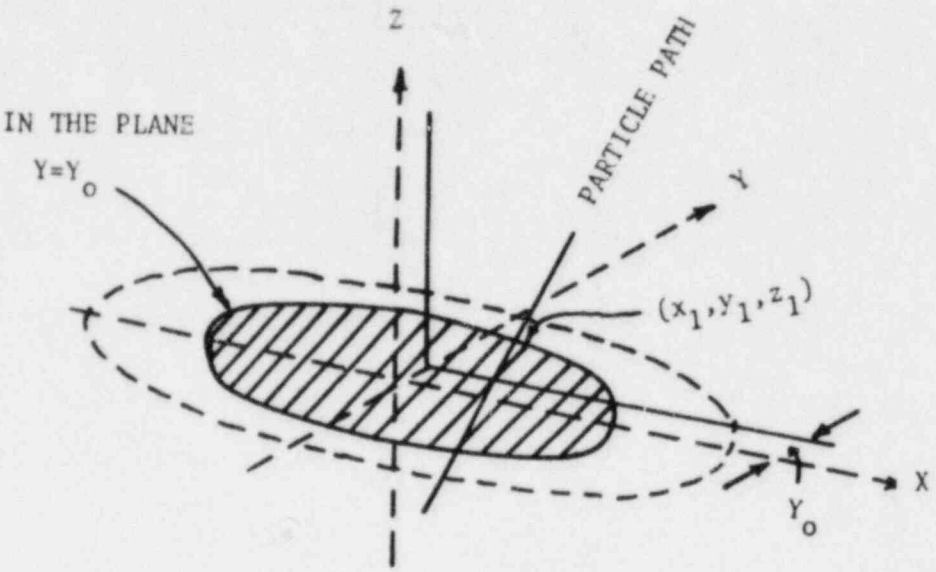

FIGURE B.1. SKETCH OF THE MEASURING VOLUME WITH THE CO-ORDINATE AXES.

The measuring volume is considered to be ellipsoidal. Let the co-ordinate axis be defined as shown in the sketch (Figure B.1). The equation of the ellipsoid is

$$\frac{x^2}{a^2} + \frac{y^2}{b^2} + \frac{z^2}{b^2} = 1 \qquad \text{(B1)}$$

The z-axis is along the measuring direction. The co-ordinates of the geometric center of the measuring volume are (0,0,0,). Let the particle path be inclined to the z axis by an angle α and contained in the plane $y=y_o$. (x_1, y_1, z_1) are the co-ordinates of the point where the particle exits from the measuring volume. (x_o, y_o) are the co-ordinates of the point of intersection of the particle trajectory and the plane of $z = 0$. (Figure B.2).

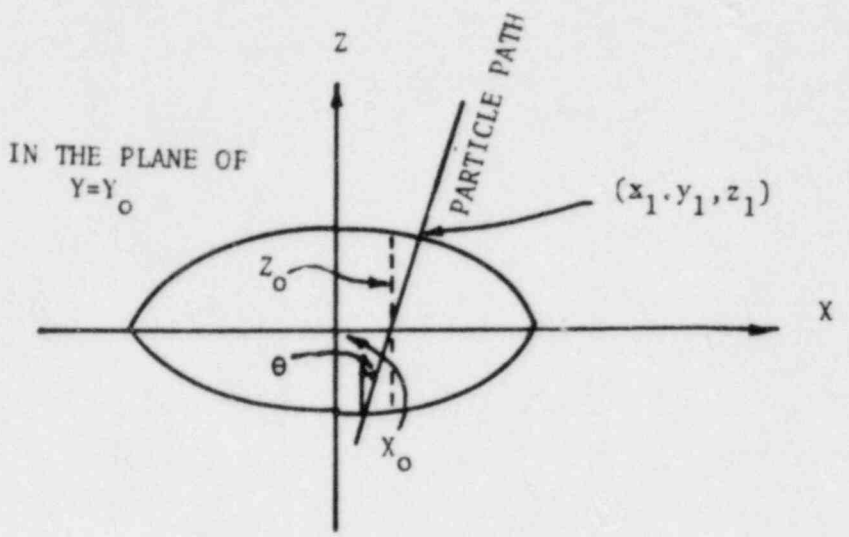

FIGURE B.2. CROSS-SECTION IN THE PLANE OF $Y=Y_o$.

$$x_1 = (x_o + z_1 \tan\theta) = x_o + \alpha z_1 \quad \text{(for small } \theta) \tag{B2}$$

$$y_1 = y_o \tag{B3}$$

Substituting Equations (B2) and (B3) in Equation (B1):

$$\frac{(x_o + 2x_o\theta z_1 + \theta^2 z_1^2)}{a^2} + \frac{y_o^2}{b^2} + \frac{z_1^2}{b^2} = 1$$

$$\left(\frac{1}{b^2} + \frac{\theta^2}{a^2}\right) z_1^2 + \left(\frac{2x_o\theta}{a^2}\right) z_1 + \left(\frac{x_o^2}{a^2} + \frac{y_o^2}{b^2} - 1\right) = 0$$

This reduces to

$$\left(\frac{1}{b^2} + \frac{2}{a^2}\right) z_1^2 + \left(\frac{2x_o\theta}{a^2}\right) z_1 - \frac{z_o^2}{b^2} = 0$$

Hence

$$z_1 = \frac{-\left(\frac{2x_o\theta}{a^2}\right) \pm \left[\left(\frac{2x_o\theta}{a^2}\right)^2 + 4\left(\frac{1}{b^2} + \frac{\theta^2}{b^2}\right)\frac{z_o^2}{b^2}\right]^{1/2}}{2\left(\frac{1}{b^2} + \frac{\theta^2}{a^2}\right)} \tag{B4}$$

Let 'ℓ' be the actual path length of the particle. The particle velocity measured is actually the component of particle velocity component (v') in z - direction and the path time measured corresponds to the total time (t) taken by the particle to pass through the measuring volume. Hence $tv' = \ell \cos \epsilon$ (Figure B.2). If the particle path was in the measuring direction the path length would be $2z_o$. Hence the error introduced is $(\ell \cos \epsilon - 2z_o)$.

From Equation (B4),

$$\ell \cos \alpha = \frac{\left[\left(\frac{2x_o\theta}{a^2}\right)^2 + 4\left(\frac{1}{b^2} + \frac{\theta^2}{a^2}\right)\frac{z_o^2}{b^2}\right]^{1/2}}{\left(\frac{1}{b^2} + \frac{\theta^2}{a^2}\right)}$$

$$= \frac{2\left(\frac{z_o}{b}\right)}{\left(\frac{1}{b^2} + \frac{\theta^2}{a^2}\right)^{1/2}}\left[\frac{\left(\frac{x_o^2\theta^2}{a^4}\right)}{\left(\frac{1}{b^2} + \frac{\theta^2}{a^2}\right)}\left(\frac{b^2}{z_o^2}\right) + 1\right]^{1/2} \qquad \text{(B5)}$$

Let $c^2 = \dfrac{\left(\frac{x_o^2}{a^4}\right)\left(\frac{b^2}{z_o^2}\right)}{\left(\frac{1}{b^2} + \frac{\theta^2}{a^2}\right)}$ and $d = \frac{b}{a}$

Equation (B5) reduces to

$$\ell \cos \alpha = \frac{2z_o\,(1 + \theta^2 c^2)^{1/2}}{(1 + \theta^2 d^2)^{1/2}}$$

$$\simeq \frac{2z_o\,(1 + \theta^2 c^2/2)}{(1 + \theta^2 d^2/2)}$$

$$\simeq 2z_o\left(1 + \frac{x_o^2\theta^2 d^4}{z_o^2}\right)$$

$$\simeq 2z_o\left[1 + \theta^2 d^4\left(\frac{x_o}{z_o}\right)^2\right] \qquad \text{(B6)}$$

Hence the error introduced is of the order of $\theta^2 d^4 \left(\frac{x_o}{z_o}\right)^2$.

Since only the central core of the measuring volume is considered, (x_o/z_o) will be a very small quantity, of the same order as θ. So the error introduced is of the order θ^4.

In another extreme case when the particle path is inclined to the z-axis but contained in the plane $x=x_o$, Equation (B6) is reduced to

$$\ell \cos\theta = 2z_o \left[1 + \theta^2 \left(\frac{y_o}{z_o}\right)^2\right]$$

since $d = \frac{b}{a} = 1$.

Still the error introduced will be of the order θ^4. Any other deviation in particle path direction will result in an error value between these two limits.

NRC FORM 335 (6 83) U.S. NUCLEAR REGULATORY COMMISSION

BIBLIOGRAPHIC DATA SHEET

1. REPORT NUMBER (Assigned by TIDC, add Vol. No., if any)
NUREG/CR-4034

2. Leave blank

3. TITLE AND SUBTITLE
A Study of Droplet Hydrodynamics Across a Grid Spacer

4. RECIPIENT'S ACCESSION NUMBER

5. DATE REPORT COMPLETED
MONTH: February YEAR: 1984

6. AUTHOR(S)
S. L. Lee, S. K. Cho and M. J. Sheen

7. DATE REPORT ISSUED
MONTH: November YEAR: 1984

8. PERFORMING ORGANIZATION NAME AND MAILING ADDRESS (Include Zip Code)
College of Engineering & Applied Sciences
State University of New York at Stony Brook
Stony Brook, New York 11794

9. PROJECT/TASK/WORK UNIT NUMBER

10. FIN NUMBER
NRC-G-04-81-014

11. SPONSORING ORGANIZATION NAME AND MAILING ADDRESS (Include Zip Code)
Division of Accident Evaluation
Office of Nuclear Regulatory Research
U. S. Nuclear Regulatory Commission
Washington, D. C. 20555

12a. TYPE OF REPORT
Technical Report

12b. PERIOD COVERED (Inclusive dates)
April 1982 to February 1984

13. SUPPLEMENTARY NOTES

14. ABSTRACT (200 words or less)

The results of measurement of droplet size and velocity upstream and downstream of the grid spacer are reported. All experiments were performed at ambient atmospheric pressure and room temperature. The Laser Doppler Anemometer (LDA) system was used for simultaneous measurement of size and velocity of a droplet, and at every measurement location two size measurement schemes were employed. These measurement results show that some of the thermally inactive large droplets (greater than 1mm) are intercepted by the grid spacer and broken down to thermally more active smaller droplets (less than 100 microns) after the grid spacer. From the obtained data, Sauter mean diameter and area density were calculated. The correlations on the Sauter mean diameter of the large and small droplets downstream of the grid spacer are reported. In addition, correlations on the fractional volume of the small droplets and nozzle characteristics are reported respectively. These results show that after liquid droplets' breakage, the total surface area of the droplets is greatly increased. This phenomena will lead to enhanced cooling of fuel rods in nuclear reactor during reflood for a postulated large loss of coolant accident.

15a. KEY WORDS AND DOCUMENT ANALYSIS

15b. DESCRIPTORS

Laser Doppler Anemometer
Droplet Breakup at Grid Spacer
Large break loss of coolant accident

16. AVAILABILITY STATEMENT
Unlimited

17. SECURITY CLASSIFICATION (This report)
Unclassified

18. NUMBER OF PAGES

19. SECURITY CLASSIFICATION (This page)
Unclassified

20. PRICE
$